INSTRUMENTATION AND MODELLING OF A REACTOR CONTAINMENT BUILDING

REPORT 2018:526

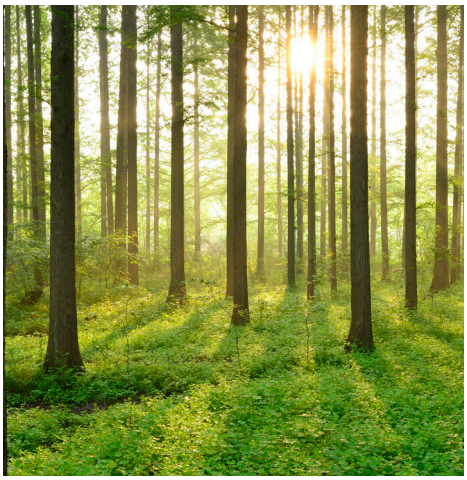

BETONGTEKNIK KÄRNKRAFT

NUCLEAR CONCRETE R&D PROGRAM

Energiforsk

Instrumentation and Modelling of a Reactor Containment Building

TOBIAS GASCH, LAMIS AHMED, RICHARD MALM

ISBN 978-91-7673-526-8 | © Energiforsk August 2018 |Cover photo TVO

Energiforsk AB | Phone: 08-677 25 30 | E-mail: kontakt@energiforsk.se | www.energiforsk.se

Foreword

The most important safety barrier in a nuclear power plant is the reactor containment, a post-tensioned concrete structure enclosing the reactor. The pre-stressing tendons prevent cracking of the concrete in case of a reactor accident, why the tension in the tendons is crucial to the integrity of the reactor containment. The tendon forces decrease over time, so to ensure the integrity of the reactor containment, it is important to monitor the tendon forces.

In this project, an instrumentation system of the reactor containment has been suggested for the Finnish nuclear power plant Olkiluoto 2, for measuring the global and local deformations of the structure, moisture and temperature. The system could be used for continuous long-term measurements and during the periodic pressure tests. The study has been carried out by PhD student Tobias Gasch, as well as senior researchers Lamis Ahmed and Richard Malm, all at The Royal Institute of Technology (KTH).

The project has been carried out in the framework of the Energiforsk Nuclear Concrete Research Program, with stakeholders Vattenfall, Uniper, Fortum, Teollisuuden Voima Oy (TVO), Skellefteå Kraft, Karlstads Energi and the Swedish Radiation Safety Authority (SSM).

Sammanfattning

Kärntekniska reaktorinneslutningar består typiskt av förspänd betong, där spännarmering används i syfte att inducera tryckspänningar i betongen och på så sätt förhindra att sprickor uppstår. Spännarmeringen utgör därmed en viktig del för att bibehålla reaktorinneslutningens strukturella integritet. I många fall injekteras spännkablarna med cementinjektering i syfte att förhindra korrosion. Detta resulterar dock i att det inte är möjligt att direkt utvärdera kablarna eller att spänna kablarna ytterligare om signifikanta långtidsförluster uppstår.

Nackdelen med cementinjekterade kablar är att det inte är möjligt att kontrollmäta spännkraftens nuvarande nivå. En konventionell metod för att bedöma inneslutningens status, och därmed indirekt spännkablarna, är att genomföra trycktester. Dessa trycktester genomförs där ett övertryck byggs upp i inneslutningen. Responsens hos inneslutningen kan därefter bestämmas baserat på töjnings- och/eller deformationsmätningar.

Syftet med föreliggande projekt är att genomföra simuleringar av trycktester på en typisk kokvattenreaktor (BWR) som förekommer i Sverige och Finland. Baserat på dessa simuleringar bestäms förväntad respons hos inneslutningen och förslag på instrumentering, så som lämplig placering och typ av givare, presenteras. Föreslagen instrumentering har kategoriserats som detektorer respektive stödinstrumentering. Detektorer avser givare som krävs för övervakning av strukturell respons av inneslutningen medan stödinstrumentering avser givare som behövs för att ta fram erforderlig indata till numeriska analyser.

Föreslagen instrumentering baseras på detektorer som placeras vid fyra vertikala positioner av inneslutningsväggen samt vid tre punkter längs omkretsen på inneslutningsväggen. Vid dessa positioner, rekommenderas att förskjutnings-givare, töjningsgivare och temperaturgivare installeras. Utöver dessa rekommenderas även övervakning av den relativa förskjutningen mellan cylinderväggen och mellanbjälklaget.

Som stödinstrumentering rekommenderas att omgivningstemperatur och relativ fuktighet mäts eftersom dessa utgör viktig indata för numeriska analyser och därmed för prediktering av strukturellt beteende.

Summary

Nuclear concrete containment buildings typically consist of pre-stressed concrete. The pre-stressing tendons are utilized to enforce a compressive state of stress to ensure that cracks do not occur in the containment structure. The tendons are thereby an important part of the containment building and important for its structural integrity. In many cases, these tendons are grouted with cement grout to prevent corrosion. This results however in that it is not possible to directly assess the tendons or re-tension these if significant long term losses occurs.

The drawback with cement grouted tendons is, thereby, that it is not possible to directly measure the current tendon force. One conventional method to assess the status of the containment building, and thereby indirectly the tendons, is to perform pressure tests. The pressure tests are performed where the pressure in the containment building is increased. The response of the containment can after this be determined based on measurements of displacements and strains.

The purpose of this project is to perform simulations of a pressure test of a Boiling Water Reactor (BWR) that is common in Sweden and Finland. Based on these simulations, the response of the containment building is determined and suggestions are made regarding suitable placement of measuring sensors. The suggested instrumentation has been divided into different types of sensors defined as detectors and support sensors. The detectors are needed to monitor the structural response of the containment while the support sensors are needed to give sufficient input to numerical analyses.

It is suggested that detector sensors are placed at four vertical positions and at three points along the perimeter. At these locations, it is recommended that displacement sensors, strain gauges and temperature sensors are installed. In addition, it is also recommended that the relative radial displacement between the intermediate slab and the cylinder wall is monitored.

As support sensors, it is recommended that the ambient temperature and relative humidity is measured since these constitute important boundary conditions for numerical analyses and thereby prediction of the structural behaviour.

List of content

1 Introduction

The concrete containment building constitutes an important part of the safety barriers of a nuclear power plant. It consists normally of thick concrete (typically 1 m) which is pre-stressed with both vertical and hoop tendons. Illustrations of typical concrete reactor containment buildings are shown in Figure 1-1. In the figure, both a Boiling Water Reactor (BWR) and Pressure Water Reactor (PWR) are illustrated.

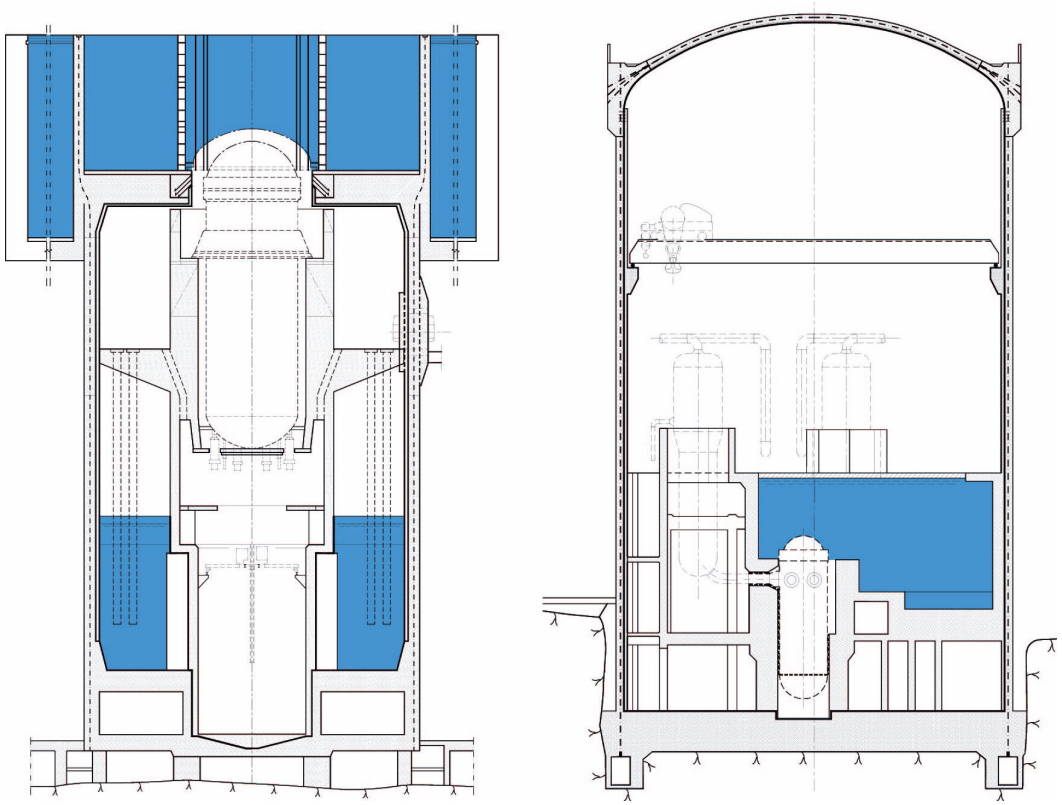

Figure 1-1: Sketch of a BWR (Forsmark I) and PWR (Ringhals III) reactor, from **[1]**.

The concrete containment building is designed to be subjected to compressive stresses during its expected service life but also due to potential accidents, such as loss of coolant accident (LOCA). The tendons reduce deformations and thereby prevent cracks in the concrete containment. In addition to this, a rather thick steel liner is placed on the inside of the containment building which should ensure that the containment building is leak tight in the event of a postulated accident conditions.

The tendons are thereby an important part of the containment building and important for its structural integrity. In many cases, these tendons are grouted with cement grout to prevent corrosion. This results however in that it is not possible to directly assess the tendons or re-tension these if significant long term losses occur.

One conventional method to assess the status of the containment building, and thereby also the tendons, is to perform pressure tests. The pressure tests are performed where the pressure in the containment building is increased for a short duration. The response of the containment can after this be determined based on measurements of displacements and strains according to alternative B in Reg. Guide 1.90, [2].

The purpose of this project is to perform simulations of a pressure test of a BWR containment that is common in Sweden and Finland. Based on these simulations, the response of the containment building is determined and suggestions are made regarding suitable placement of measuring sensors. The suggested amount of sensors that are given corresponds to a lower limit of sensors that should be used to capture the behaviour of the containment. The suggested amount of sensors also includes some redundancy in order to be able to detect possible errors with sensors and to be able to capture the response of the even if a few sensors would malfunction.

The intention of this report is that the concept can be utilized for different BWR reactors. However, the models developed in this project are based on input from the reactor Olkiluoto 2 provided by TVO.

1.1 LIMITATIONS

The containment used as basis for this study is the Olkiluoto 2 containment building. Limited information has been available during this project, and therefore several assumptions have been made. For instance, it is only the structural concrete and tendons in the cylindrical containment building that has been implicitly included in the analyses. The effect from the pools have been considered by added masses and restraint conditions in the top. The reinforcement has not been included in the analyses since the reinforcement has no influence on the behaviour of the concrete as the containment is uncracked and considered to be linear elastic. The liner is not considered to be a load carrying component and has been excluded from the analyses. In addition, some material properties were not available and therefore estimated. A description of the assumptions made in the report are further described in Chapter 2. These simplifications have been made since they has minor or no influence on the results for this project. Despite that all information has not been available, all assumptions regarding material properties have been made as average values and should, therefore, be representative for the typical BWR containment buildings in Sweden and Finland.

Two simplified numerical finite element models (an axi-symmetric and a ring model) were developed in this project to evaluate the influence of the containment wall during pressure tests.

1.2 METHOD

The initial plan was to use a previously developed 3D FE-model of the containment building for this project. However, it was not possible to utilize this for the purposes of this project.

Therefore, two alternative models (an axi-symmetric and a ring model) were developed instead. The axi-symmetric model calculated the 3D behaviour of the containment wall based on the average behaviour of the containment building without respect to the variation in wall thickness at the anchoring of tendons etc. The ring model also calculates the 3D behaviour, but only for a slice of the containment wall. The ring model is able to capture the uneven radial displacement over the perimeter of the containment wall due to variation in thickness. Two different ring models were developed for two altitudes of the containment wall.

1.3 ACKNOWLEDGEMENT

The authors are thankful for all material that has been provided regarding Olkiluoto 2 (OL2) by the curtesy of Teollisuuden Voima Oyj (TVO).

2 Olkiluoto 2

2.1 GEOMETRY

The overall geometry of the containment structure at Olkiluoto 2 is shown in Figure 2-1 taken from the model report in the CONTANA-project [3]. More detailed dimensions of the idealized geometries used in the respective model are described in Section 4.1 for the axisymmetric model and Section 5.1 for the ring model.

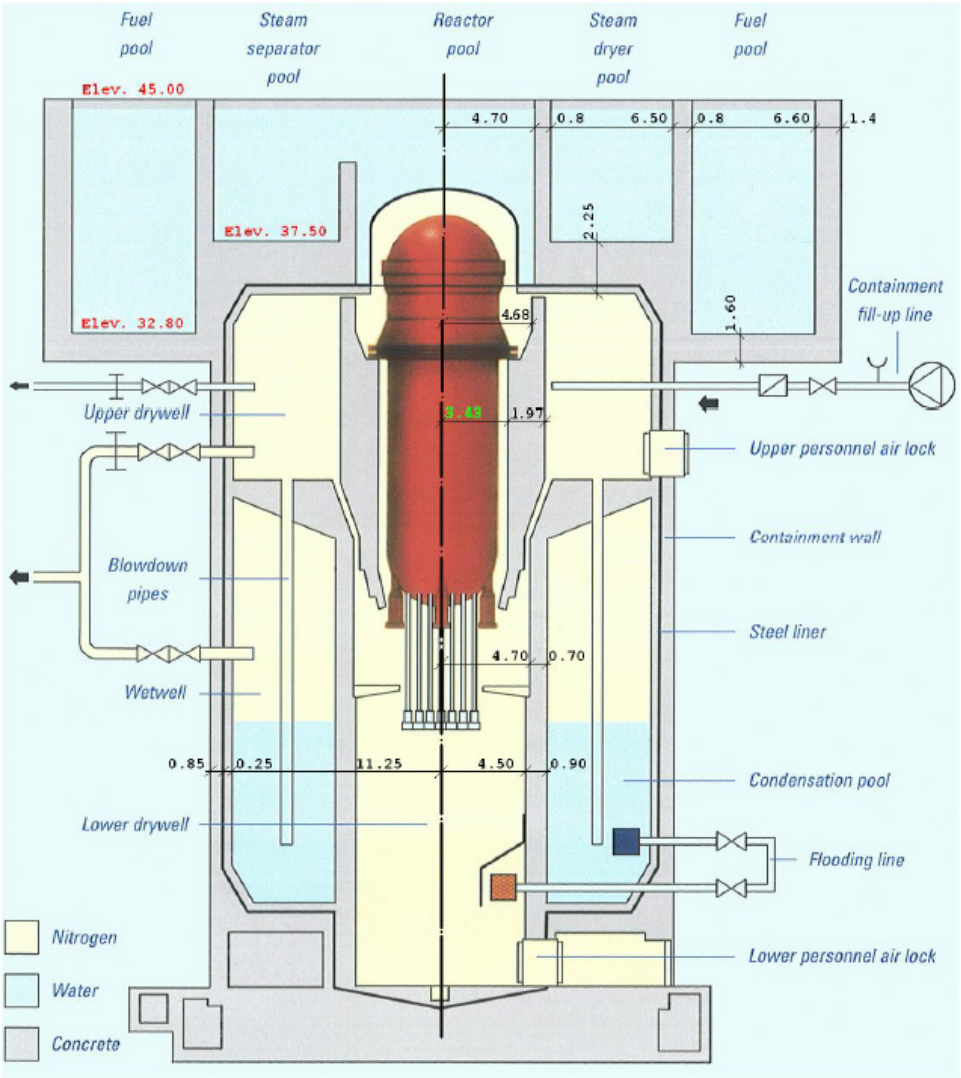

Figure 2-1: *The overall geometry of OL2 including main dimensions* **[3]**.

2.1.1 Tendons

All tendons are made of bundles of strands; each with a diameter of 6 mm. A summary of the vertical and horizontal tendons follows below.

Vertical tendons

The vertical tendons are passively anchored in the bottom of the containment and actively anchored in the top, i.e. post-tensioning is done from the top anchor point. In summary, it can roughly be said that they are evenly distributed but with additional tendons in the four areas where horizontal tendons are anchored. Table 2-1 presents a summary of the different type of tendons used and the number of tendons of each type. The total force in the vertical tendons is 14400 MP, according to the construction drawings 201-32-011.

Table 2-1: Summary of vertical tendons from drawing 201-32-002.

	No. strands/tendon	**No. tendons**	**Area [m²]**
	72	35	0.0713
	78	14	0.0309
	115	12	0.0390
Total		60	0.1411

Horizontal tendons

The horizontal tendons are anchored in two buttresses that run along the height of the containment wall. Both ends are actively anchored in one of the two buttresses, i.e. each tendon runs along the entire circumference of the containment. Tendons then alternate between the buttresses to obtain an even distribution of pre-stress. Table 2-2 presents a summary of the different type of tendons used and the number of tendons of each type. The total force in the horizontal tendons is 16600 MP, according to the construction drawings 201-32-011.

Table 2-2: Summary of horizontal tendons from drawings 201-32-002, 201-32-008 and 201-32-009.

	No. strands/tendon	**No. tendons**	**Area [m²]**
	72	122	0.2484

In addition, the horizontal tendons are placed in two layers with the radius 11.7 m and 11.9 m for the inner and outer layers, respectively. The pre-stressing force will vary along the tendon due to pre-stressing losses, such as curvature friction and wobbling. During pre-stressing, a hydraulic jack is used to tension the tendon and thereby making it elongate and slide towards the active end. This result in that frictional force develops along the length of the tendon, where the tendon force is reduced from its maximum value at the active anchor end. In this case, the tendons are tensioned at both ends and thereby the force distribution along the tendons is symmetrical, which means that the lowest tendon force is obtained in the middle of the tendon. According to Eurocode 2 (EN 1992-1-1, 2010), the pre-stressing force can be calculated as shown in Eq. 2.1

$$F(x) = F_{max} e^{-\mu(\theta + kx)} \qquad (2\text{-}1)$$

where, $F(x)$ is the variation in pre-stress from the active anchor [N]

F_{max} is the maximum tendon force, typically at the active anchor [N]

θ is cumulative sum of the change in angle [rad]

μ is the friction coefficient between the tendon and the tendon duct [-]

k is the wobble effect, i.e. the unintentional change in angle for a grouted tendon [-]

x is the distance along the tendon from the point where the maximum tendon force (F_{MAX}) occur [m]

Estimated forces for one tendon

A calculation of tendon force has been performed to estimate the average tendon force along the containment wall. The tendons are arranged in two layers, and therefore a calculation is performed on the average radius of the two layers, i.e. R = 11.8 m. Only limited information about the details of the used tendons were available in this project, therefore several parameters such as friction coefficient, wobbling, tendon force after seating had to be assumed based on typical values for these types of tendons, based on.

Table 2-3: Input to the calculation of pre-stress.

Parameter	Description	Value
μ	Friction coefficient	0.17
k	Wobbling	0.0088
R	Radius	11.8 m
F_0	Tendon force at anchor before seating	2494 kN
F_1	Tendon force at anchor after seating	0.915 F0
A	Tendon area	0.002 m^2
E	Elastic modulus of the tendon	195 GPa

As the tendon is tensioned at the active ends it will obtain a force distribution as shown in Figure 2-2. Both the initial variation in tendon force and the variation in tendon force after seating are shown. As seen in the figure, the initial part of the tendon has a small reduction in tendon force due to the friction loss due to wobbling. The remaining part of the tendon which is curved is subjected to larger losses due to both curvature friction and wobbling.

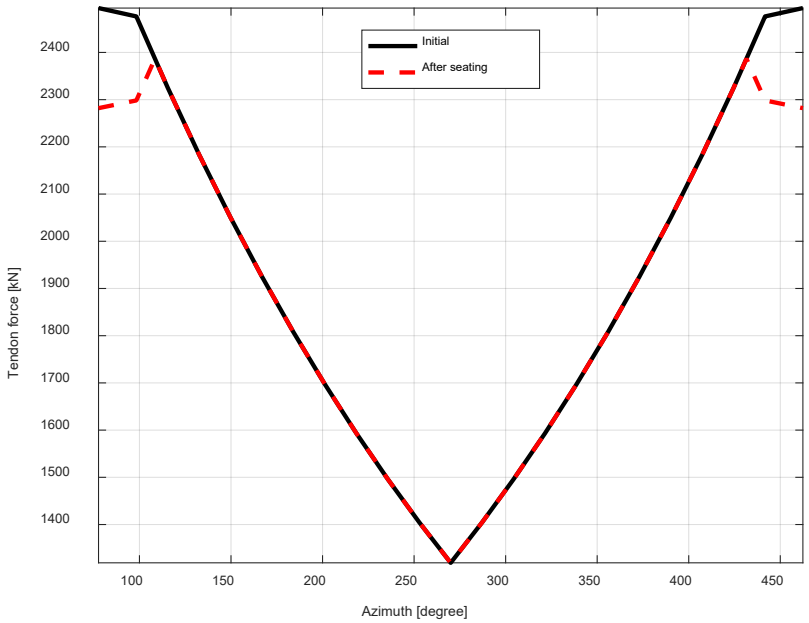

Figure 2-2: *Calculated variation in tendon force.*

As it can be seen in the figure, the maximum tendon force is about 2.387 MN after seating and it occurs about 7.1 m from the active anchor. The tendon force at the anchor of 2.387 MN after seating corresponds to a slip equal to 2.9 mm. The average force along one tendon is 1.882MN, but due to high friction and the length of the tendon, the variation in pre-stressing force is quite large where the lowest tendon force is 1.319 MN corresponding to an average loss of 6.5 %.

Estimated tendon forces along the cylinder wall

The average tendon force when two tendon (tensioned from opposite anchors) are considered is shown in Figure 2-3. However, it is reasonable to assume that a rather high variation in stress may occur along the cylinder wall. Since each tendon covers the entire perimeter of the containment and the tendon thereby overlap at the buttresses. This caused a high variation in stress along the cylinder wall at the buttresses. In order to illustrate that, an additional calculation of the overlapping is presented in Figure 2-4. As it can be seen in the figure, the average force along the cylinder wall is varying within a high interval, between 1.862 MN and 2.989 MN only near the buttresses due to the overlapping where three tendons are considered, otherwise variation interval is between 1.836 MN and 1.898 MN along the wall further away from the buttresses.

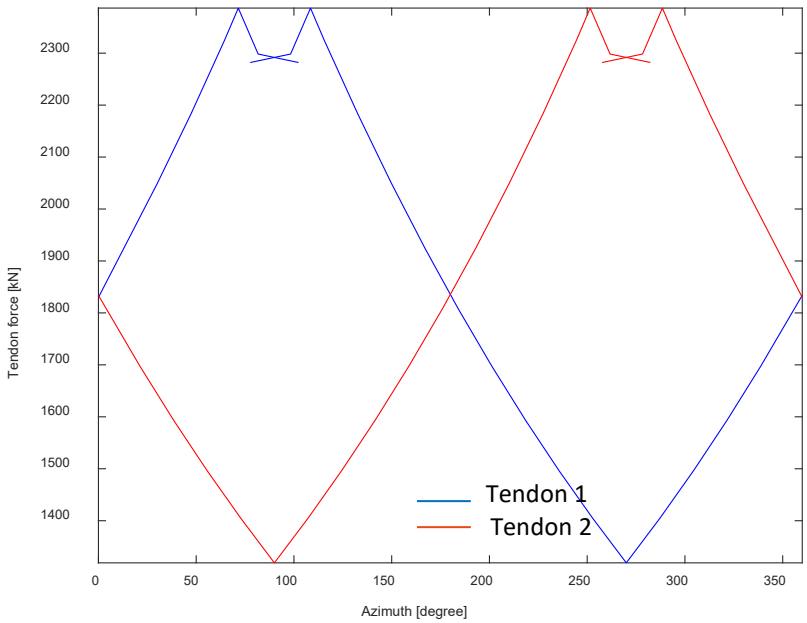

Figure 2-3: *Average tendon force along the cylinder wall.*

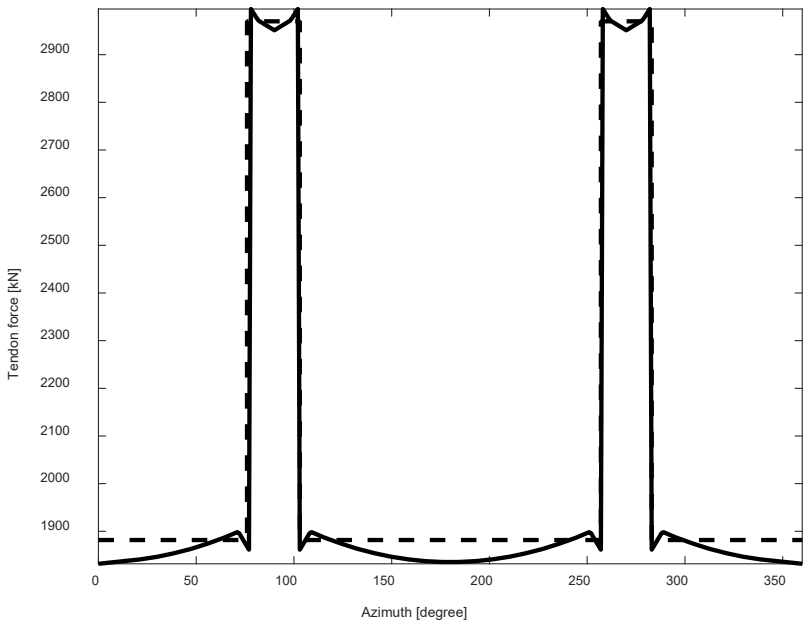

Figure 2-4: *Calculated variation in tendon force along the cylinder wall. The dashed line corresponds to using the mean value, while the solid line corresponds to using the real variation in stress along the tendons.*

2.2 MATERIAL PROPERTIES

The concrete used during the casting of OL2 was specified to correspond to a K40, but in recent measurements has been found have a compressive strength around

70 MPa. All prediction models used in this study are based on the 28 day compressive strength which is here assumed as 40 MPa. The concrete material properties have rather low influence of the results since the analyses are based on linear elastic behaviour. A summary of the used concrete properties is given in Table 2-4.

Table 2-4:.Material properties of the concrete.

Property			**Unit**	**Comment**
Mean compressive strength	f_{cm}	40	MPa	
Mean elastic moduli	E_{cm}	33.35	GPa	Calculated from f_{cm} using EC2 [4]
Poisson's ratio	ν_c	0.2	-	
Density	ρ_c	2400	kg/m^3	
Thermal exp. coefficient	α_c	10^{-5}	1/K	
Thermal conductance	λ_c	1	W/(m*K)	

The material properties used for the tendons are given in Table 2-5 and for the rock in Table 2-6. The properties of the rock are assumed and only aids in providing a better boundary condition in the axisymmetric model and have little influence on the results.

Table 2-5:.Material properties of the tendons.

Property			**Unit**	**Comment**
Mean elastic moduli	E_s	210	MPa	
Density	ρ_s	7800	kg/m^3	
Thermal exp. coefficient	α_s	10^{-5}	1/K	

Table 2-6:.Material properties of the rock.

Property			**Unit**	**Comment**
Mean elastic moduli	E_r	35	MPa	
Poisson's ratio	ν_r	0.2	-	
Density	ρ_r	2650	kg/m^3	
Thermal exp. coefficient	α_r	10^{-5}	1/K	
Thermal conductance	λ_r	1	W/(m*K)	

2.3 LOADS AND AMBIENT CONDITIONS

Only limited information about the actual temperature conditions at OL2 has been available during the project, where the temperatures in a few points inside the concrete have been measured near the outside of the containment wall. No measurements regarding ambient temperatures have been available and especially inside the concrete containment building. Therefore, temperature conditions are taken from a case study on thermally induced stresses at Forsmark F1 by Könönen [5]. The temperatures used in [5] are shown in Figure 2-5a as a reference case and those used in the current study in Figure 2-5b. However, after completion of the

report, TVO provided information that the temperature in the wet-well was 45 °C instead of the assumed temperature of 35 °C. Considering that the purpose of these analyses are to predict linear the response during a pressure test, then this deviation has no influence on the predicted results.

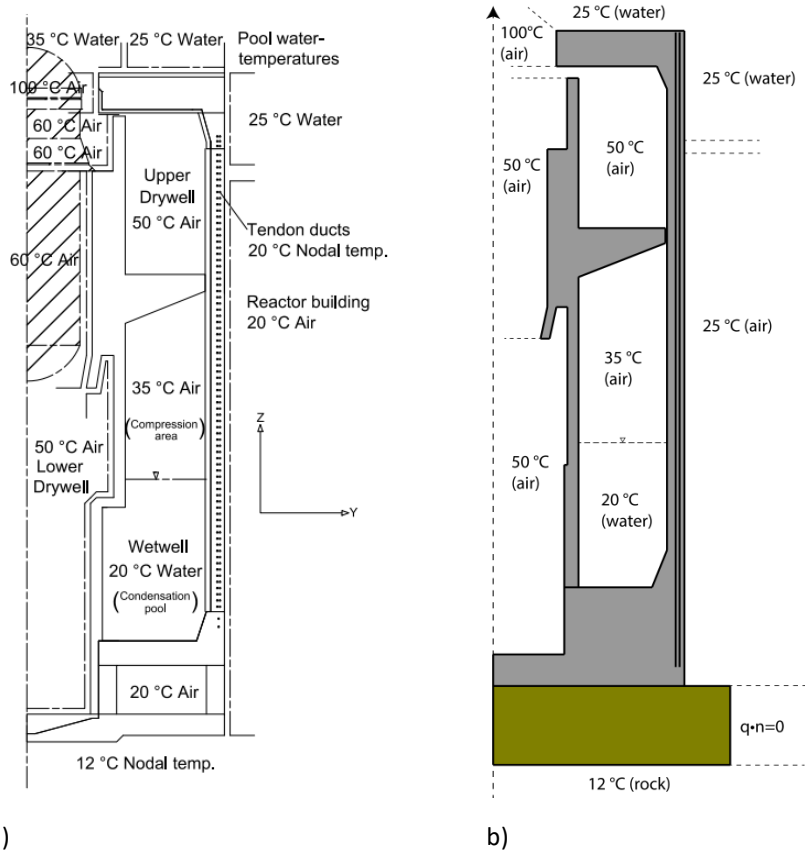

Figure 2-5: *Temperature distribution used by Könönen* **[5]** *(a) and the current study b)*.

Similarly for the mechanical loads, assumptions are based on the work of Könönen [5] who calculated equivalent pressure loads acting on the containment structure due to the weight of spent fuel pool and reactor tank for Forsmark F1, see Figure 2-6a. The figure also shows the boundary conditions used by Könönen. The loads used in the current study are shown in Figure 2-6b, all loads included in the figure is considered to be permanent. It can be noticed that slightly different boundary conditions are used compared to Könönen. Also, a different modelling strategy is used for the modelling the tendons, described in section 3.3.2, compared to Könönen who modelled the pre-stress as an external load.

An additional load not included in Figure 2-6b is the pressure load during a leak tightness test. This load is applied as a pressure load of 3 bar acting on all internal surfaces of the containment. The pressure test has typically a duration of 24 h, but may vary to some extent. It generally consists of a pressure increase during 6 h, a constant pressure during 12 h and a pressure decrease during 6 h.

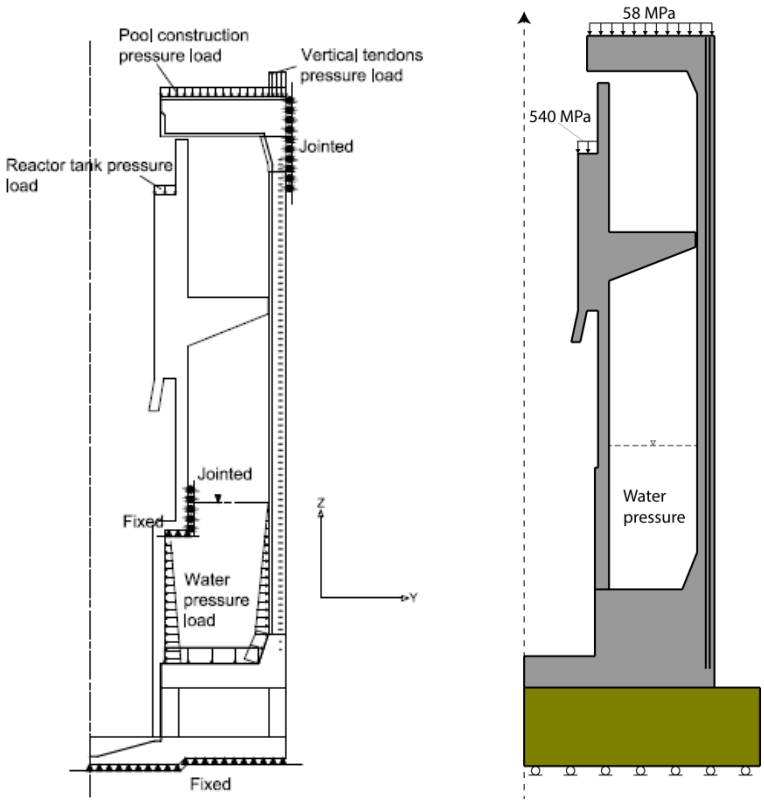

Figure 2-6: *Loads and boundary conditions used by Könönen* **[5]** *(b) and the current study (b)*.

3 Modelling

Two different types of simplified models of the containment structure at OL2 are used in this study. The purpose and differences of these two models are described in a broad sense in Section 3.1 while more details and results are given in Section 4 and 5. A general description the mathematical structure of the employed analysis method is described in Section 3.2 and 3.3 together with some other aspects of the finite element modelling relevant to both models. All equations described in the following are discretized and solved within the context of the Finite Element Method (FEM) as implemented in the general software package Abaqus [6].

3.1 SPATIAL DESCRIPTION

As mentioned, two simplified models are used to evaluate the overall behaviour of the containment structure since no 3D-model has been available during the project that could be used for the analyses. These two models only include the structural concrete and the tendons, whereas other details such as reinforcement and the steel liner are excluded. The first model is made under the assumption of axial symmetry and is intended to capture the behaviour of a typical vertical cross-section of the containment. In a model using this assumption some aspects of the real behaviour of the containment are disregarded, for example the stiffening influence of the spent fuel pool and the buttresses as well as various personnel and equipment penetrations. The three-dimensional illustration shown in Figure 3-1 is swept from such a cross-section. A more detailed description of the axisymmetric model and the results from the simulation are presented in Section 4.

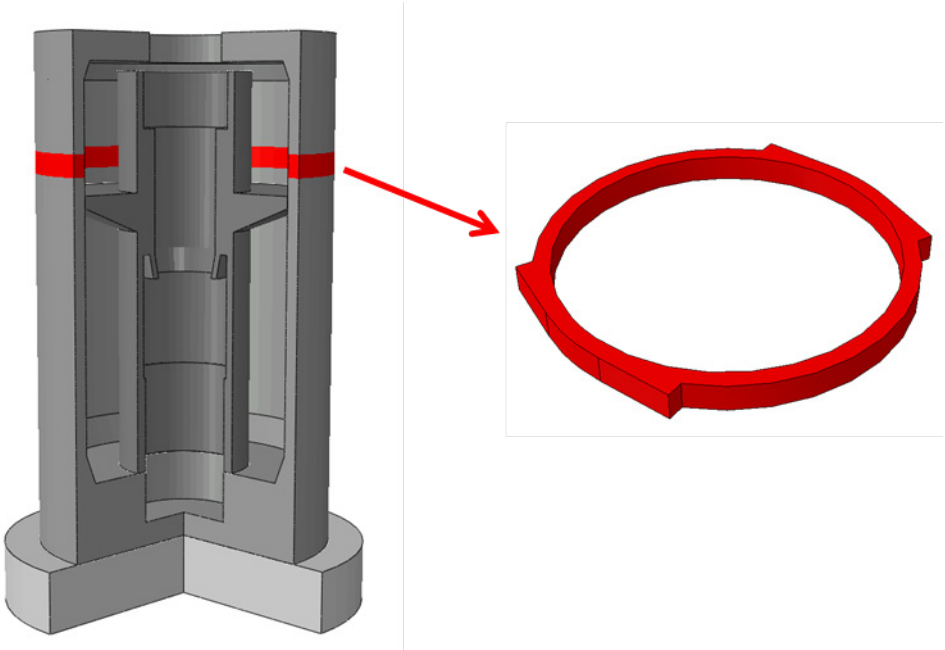

Figure 3-1: *Schematic description of the axisymmetric model in the ring model (red).*

Given that the cross-section of the cylindrical wall in reality does not comply with the assumption of axial symmetry, an additional model is made to study the three dimensional deformation of the outer containment wall. This model is constructed from a slice of the wall, schematically shown in red in Figure 3-1. Using such a model, the effect of for example the two buttresses in which tendons are anchored can be accounted for. To account for the self-weight of the part of the structure above the ring slice, a vertical pressure can be extracted from the axisymmetric model at the chosen height. A more detailed description of the ring model and results from the simulation is presented in Section 5.

3.2 THERMAL ANALYSIS

Only steady-state distributions of the temperature T are of interest in this project. These are calculated using the heat equation in Eq. (3-1), where all time-dependent terms have been omitted. In the simplified form in Eq. (3-1), the thermal material behaviour is given directly by the linear thermal conductivity λ.

$$\nabla \cdot (-\lambda \nabla T) = 0 \qquad (3\text{-}1)$$

Most surfaces in the analysed structure are in contact with either air or liquid water. Hence, to obtain a representative internal distribution of the temperature convective type boundary conditions on the form in Eq. (3-2) are used. The inward temperature flux normal to the surface on the right hand side is then controlled by the temperature difference between the surface T and the ambient medium T_{amb} in combination with the heat transfer coefficient h_T.

$$-\mathbf{n} \cdot (-\lambda \nabla T) = h_T (T_{\text{amb}} - T) \qquad (3\text{-}2)$$

Regarding the heat transfer coefficient, it is for air set to 5 W/(m²K) and for water to 200 W/(m²K). Given that only steady-state temperature distributions are desired, neither the conductivity λ nor the heat transfer coefficient h_T have significant influence on the results. The distributions will always be linear but the two properties will affect the difference between the surface temperature and T_{amb}.

Two additional descriptions of boundary conditions are required. At symmetry sections (e.g the axial symmetry or vertical surfaces in the ring model), the surface flux is set to zero. Finally, in the axisymmetric model a part of the rock is included in the model; at the far boundary of this domain the temperature is directly prescribed.

3.3 MECHANICAL ANALYSIS

Also for the mechanical part of the model, only steady-state or static results are of interest. Hence, the deformational behaviour of the structure is given by the mechanical equilibrium equation (3-3) where stresses $\boldsymbol{\sigma}$ are in balance with the body forces **b.** A small displacement formulation of the mechanical behaviour is used through the kinematic relation between strains $\boldsymbol{\varepsilon}$ and displacements **u** shown in Eq. (3-4).

$$\nabla \cdot \boldsymbol{\sigma}(\boldsymbol{\varepsilon}) - \mathbf{b} = 0 \qquad (3\text{-}3)$$

$$\boldsymbol{\varepsilon} = \frac{1}{2}[\nabla \mathbf{u} + (\nabla \mathbf{u})^{\mathrm{T}}] \quad (3\text{-}4)$$

Equations (3-3) and (3-4) are complemented with boundary conditions to fully describe the mechanical behaviour. Either fluxes (loads) or prescribed displacements are prescribed on surfaces. More information on the exact boundary conditions used is given in connection to the respective model in Section 4 and 5.

3.3.1 Material behaviour

The final equations needed to complete the mechanical model used are constitutive equations to relate stresses and strains for each material used. The form of constitutive equation used for concrete, tendons and rock are described in the following. All time-dependent properties such as creep in the concrete and relaxation in tendons are calculated at an age of 35 years and pre-stressing is assumed to take place 1 year after casting. No transient results are considered, thereby only the state of the structure after 35 years is presented.

Concrete

The form of the constitutive equation for concrete is given in Eq. (3-5). Stresses in all concrete parts are directly proportional to the elastic deformations calculated with Hooke's law using the elasticity tensor **D**. The elastic behaviour is thus controlled by two material constants: Young's modulus E_c and Poisson's ratio ν_c. Elastic deformations are defined as the total strain $\boldsymbol{\varepsilon}$ minus the deformation caused by creep ε_{cr}, shrinkage ε_{sh} and thermal expansion ε_{th}.

$$\boldsymbol{\sigma} = \mathbf{D}(E_c, \nu_c) : (\boldsymbol{\varepsilon} - \varepsilon_{cr}\mathbf{I} - \varepsilon_{sh}\mathbf{I} - \varepsilon_{th}\mathbf{I}) \quad (3\text{-}5)$$

Creep and shrinkage strains in the concrete are calculated using the cross-sectional approach with the model prescribed in the Eurocode 2 [4]. The model is summarized in the following. Starting with the description of creep, it is calculated using a time dependent creep ratio φ. The creep ratio is in the EC2 model dependent on the age of concrete at loading t_0, the compressive strength of the concrete and the ambient relative humidity. A detailed description of how φ is calculated is given in appendix A. Once φ is calculated for $t = 35$ years, the creep strain ε_{cr} is given by Eq. (3-6) where σ_c is the compressive stress in the concrete.

$$\varepsilon_{cr}(t) = \frac{\varphi(t, t_0)\sigma_c}{E} \quad (3\text{-}6)$$

Calculating creep for general stress conditions require a viscoelastic formulation in a form similar to that described by Gasch et al. [7] which is out-of-scope of the current investigation. Instead creep is only considered in areas where pre-stress is present (i.e. the cylinder wall) where stresses from the pre-stress are dominant. Hence in these areas σ_c in Eq. (3-6) is set equal to the equivalent concrete stress from the pre-stress in the vertical and tangential directions while all other components are kept at zero. Also in all other areas not affected by pre-stress, σ_c is kept at zero.

Shrinkage strains ε_{sh} are in EC2 [4] decomposed in two parts as in Eq. (3-7): drying shrinkage ε_{cd} and autogenous shrinkage ε_{ca}. Given that all concrete surfaces in the

containment are coated with a moisture tight epoxy barrier, no drying shrinkage occurs, i.e. $\varepsilon_{cd} = 0$.

$$\varepsilon_{sh} = \varepsilon_{cd} + \varepsilon_{ca} \quad (3\text{-}7)$$

Autogenous shrinkage is in [4] calculated according to Eq. (3-8) where the factor β_{as} controls its evolution in time and ε_{ca} is its asymptotic value (i.e. at complete hydration). See appendix A for further details and note that only the value of $\varepsilon_{ca}(t)$ at $t = 35$ years is used in the simulations presented in the following chapters.

$$\varepsilon_{ca}(t) = \beta_{as}(t)\varepsilon_{ca}(\infty) \quad (3\text{-}8)$$

Thermal strains ε_{th} are assumed linearly dependent on the temperature state following Eq. (3-9) where α is the constant linear coefficient of thermal expansion and T_{ref} is a reference temperature at which the material is stress/strain free. The temperature T is taken from as the spatial field calculated in the thermal analysis described in Section 3.2.

$$\varepsilon_{th} = \alpha_c\left(T - T_{ref}\right) \quad (3\text{-}9)$$

The reference temperature T_{ref} is here set to 20 °C which corresponds to the assumed temperature in the reactor building surrounding the containment, see Figure 2-6.

To exemplify the inelastic strains in the concrete, the time evolution of creep and shrinkage is shown in Figure 3-2. Note again that only the discrete values calculated at $t = 35$ years are used in the simulations in sections 4 and 5 since transient and non-linear effects are not included in the model equations.

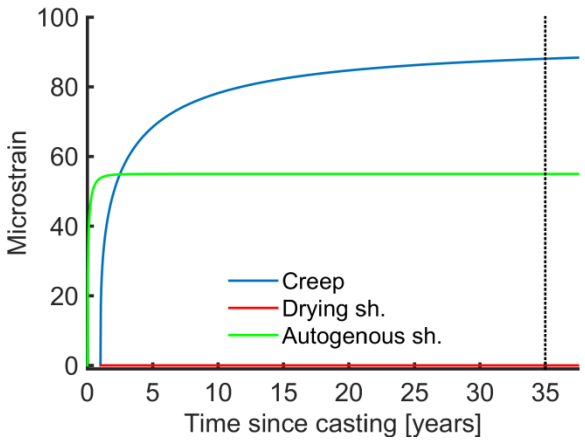

Figure 3-2: *Creep and shrinkage calculated using the EC2 model* **[4]**.

Steel

The constitutive behaviour of the steel tendons is given in Eq. (3-10) on a similar form as for the concrete. However, a major difference in the elastic behaviour is that the tendons are assumed to behave as a one-dimensional material. Hence the elasticity tensor **D** reduces to single material constant; Young's modulus E_s. As will

be described in more detail in sections 4 and 5, tendons are in the axisymmetric model included as a membrane with stiffness in only one direction; vertical or tangential. In the ring model, tendons are modelled as trusses.

$$\sigma = E_s\left(\varepsilon - \varepsilon_{pi} - \varepsilon_{pr} - \varepsilon_{th}\right) \qquad (3\text{-}10)$$

The elastic deformations are again given as the total strain ε minus some inelastic deformations. For the steel these are instantaneous strain ε_{pi} due to the prescribed pre-stress force, losses due to relaxation ε_{pr} and thermal strains ε_{th}. The instantaneous strain depends on where in the containment the tendon is located, and the thermal strains are calculated using Eq. (3-9). The relaxation strains ε_{pr} are given in Eq. (3-11) where the loss in pre-stress $\Delta\sigma_{\mathrm{pr}}$ is calculated as in the EC2 [4] with a relaxation loss of 2.5 %, see appendix A for further detail.

$$\varepsilon_{pr} = \frac{\Delta\sigma_{pr}}{E_s} \qquad (3\text{-}11)$$

Rock

The constitutive behaviour of the rock is given in Eq. (3-12) on a similar form as for the concrete. The isotropic elastic behaviour is given by the two material constants E_r and ν_r and only one inelastic strain is considered; thermal strains ε_{th}. Notice that the rock is only included in the axisymmetric model in Section 4.

$$\boldsymbol{\sigma} = \mathbf{D}(E_r, \nu_r) : (\boldsymbol{\varepsilon} - \varepsilon_{th}\mathbf{I}) \qquad (3\text{-}12)$$

3.3.2 Modelling pre-stress of tendons

Modelling of pre-stress in the tendons require some additional attention. The tendon system at OL2 is grouted, meaning that it fully interacts with the surrounding concrete. Additionally, after the first post-tensioning, no re-tensioning is possible at a later stage to compensate for losses. With this in mind, modelling of the tendons requires some new assumptions apart from those related to the material behaviour previously described:

1. All autogenous shrinkage has occurred before post-tensioning of the tendons
2. Before post-tensioning, the tendons have no strain but follow the deformation of the concrete
3. During and after post-tensioning, the tendons are perfectly constrained to the concrete

To account for these three assumptions, the tendons in the simulations assumed inactive until post-tensioning at which time they are reactivated with zero strain. This is achieved using the `*Model Change` functionality available in Abaqus [6]. The sequence in which the tendons are deactivated and reactivated with respect to the other loads considered is described in the next section.

3.3.3 Analysis sequence

As mentioned earlier, time is not explicitly considered as a variable in the analyses. However, the sequence in which effects and loads are applied is important whence

a pseudo-time is included in the mechanical analyses. The analyses include six steps that define the sequence in which loads are applied, where each step corresponds to one unit of pseudo-time. The steps are summarized as:

0. Initial conditions: $\mathbf{u} = 0$ and $T = T_{\text{ref}}$
   Tendons are deactivated

1. Self-weight applied: $\mathbf{b} = \rho\mathbf{g}$
   Weight of reactor tank and spent fuel pool applied as loads, see Figure 2-6.

2. Autogenous shrinkage ε_{ca}(35 years)

3. Tendons are reactivated
   Instantaneous strain ε_{pi} due to pre-stress applied to tendons

4. Concrete creep ε_{cr}(35 years) and relaxation in tendons ε_{pr}

5. Temperature field from thermal analysis is applied

6. Internal pressure of 3 bars corresponding to pressure test is applied to all internal surfaces of the containment.

4 Axi-symmetric models

As mentioned in Section 3, to study the overall behaviour of the outer containment wall, an asymmetrical model using a simplified cross-section is employed. This model is intended to capture the global behaviour of the structure but will not be able to model localized effects close to for example equipment hatches nor three-dimensional effects due to for example the spent fuel pool. In this section some special modelling aspects related to the asymmetrical model is described and the results of the simulation presented.

4.1 GEOMETRY

The main dimension of the axisymmetric cross-sections is taken from the report [3] and complemented with some measurements from drawings provided during the project. Given the nature of an axisymmetric model, some features of the actual geometry cannot be included in the model since they are three-dimensional such as:

- Spent fuel pool
- Tendon galleries and buttresses
- Equipment and personnel hatches

The geometry of the used cross-section is shown in Figure 4-1a, and a swept three-dimensional representation in Figure 4-1b. The model includes a rock slab under the containment structure to obtain a better representation of the boundary conditions, in both the thermal and mechanical analyses.

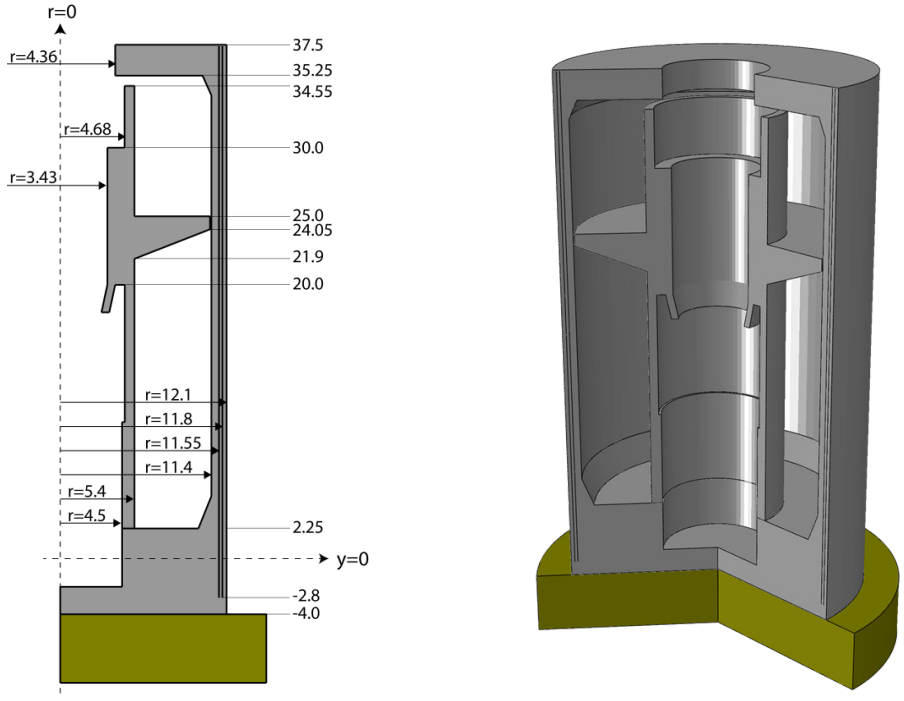

Figure 4-1: *Axisymmetric geometry (a) and 3D representation (b).*

4.1.1 Tendon equivalent membranes

To model the tendons in an axisymmetric setting, two membranes are included in the model, one corresponding to vertical tendons placed at a radius of 11.55 m and one corresponding to the horizontal tendons placed at a radius of 11.8 m (i.e. the mean radius of horizontal tendons). To account for the actual cross-sectional area of the tendons, an equivalent thickness is calculated based on the total areas reported in Table 2-1 and Table 2-2. The equivalent thickness t_v of the membrane representing the vertical tendons is calculated using the mean radius r_v of the tendon membrane as:

$$t_v = \frac{A_v}{2\pi r_v} = \frac{0.1411}{2\pi \cdot 11.5} = 0.0019 \text{ m} \qquad (4\text{-}1)$$

Similarly, the equivalent thickness t_h of the membrane representing the vertical tendons is calculated using the height of the membrane which is equal to 40.2 m. This gives:

$$t_h = \frac{A_h}{40.2} = \frac{0.2484}{40.2} = 0.0062 \text{ m} \qquad (4\text{-}2)$$

4.2 BOUNDARY CONDITIONS AND LOADS

4.2.1 Thermal

Temperature boundaries are defined according to Figure 2-5. All temperature boundary conditions are defined using Eq. (3-2), except at the bottom of the rock domain where the temperature is directly prescribed at the boundary. Furthermore, the heat flux is set to zero at symmetry boundary.

4.2.2 Mechanical

Boundary conditions

The only parts of the model with prescribed displacement are the rotational symmetry line and the outer surface of the rock domain. The displacements for these surfaces/lines are prescribed to zero in their normal direction.

In addition, the bottom of the containment is fully constrained to the rock domain.

External loads

The applied external loads are listed below; their background is described in Section 2.3. All loads are applied during the self-weight (1) described in Section 3.3.3, except the internal pressure.

- Fuel pool – Weight of 58 kPa applied to the top surface of the containment
- Condensation pool – Hydrostatic pressure from a water depth of 6.75 m
- Reactor tank – Weight of 540 kPa applied to the reactor tank support
- Leak tightness test – Internal pressure of 3 bars applied to all surfaces inside the containment

Internal loads

Temperature is taken from the thermal analysis to calculate the thermal strains ε_{th} needed in the constitutive equations presented in Section 3.3.

The instantaneous strain ε_{pi} needed in constitutive equation (3-10) for the tendons in the respective tendon direction, is calculated as:

$$\varepsilon_{pi,v} = \frac{F_{v,tot}}{A_v E_s} = \frac{14400 \cdot 9810}{0.1411 \cdot 210e9} = 0.048 \qquad (4\text{-}3)$$

$$\varepsilon_{pi,h} = \frac{F_{h,tot}}{A_h E_s} = \frac{16600 \cdot 9810}{0.2884 \cdot 210e9} = 0.0031 \qquad (4\text{-}4)$$

where the forces $F_{v,tot}$ and $F_{h,tot}$ are taken as the average forces without considering long-term losses. Also, using the equation from EC2 [4] (presented in appendix A) to calculate the loss in pre-stress due to relaxation yields:

$$\Delta\sigma_{pr,v} = 29.6 \text{ MPa} \qquad (4\text{-}5)$$

$$\Delta\sigma_{pr,h} = 6.4 \text{ MPa} \qquad (4\text{-}6)$$

As already discussed in Section 3.3.1, the compressive stress σ_c needed in Eq. (3-6) is estimated from the FE analysis and taken as an approximate stress in the containment wall directly after the post-tensioning. Given the different amounts of pre-stress in the vertical and horizontal directions two stresses are taken from the model:

$$\sigma_{c,v} = 2.7 \text{ MPa} \qquad (4\text{-}7)$$

$$\sigma_{c,h} = 3.5 \text{ MPa} \qquad (4\text{-}8)$$

resulting in different amounts of creep for the respective direction. To this end it must be emphasized that these are approximate stresses that are assumed uniform in the entire wall. In the simulation as well as in reality, stresses in the containment wall are not uniform due to its deformation, temperature and shrinkage effects. However, stresses due to the pre-stress are dominating and the approximation gives satisfactory results for the purpose of this study.

4.3 MESH

The concrete containment structure is discretized using triangular elements with second-order shape functions and an approximate size of 0.2 m. The tendon membranes are discretized with elements with the same approximate size. The rock domain is as the containment structure discretized with triangular elements both an approximate size of 0.2 m is only kept close to the containment structure; the element size then increases up to 1 m at the far boundary. These mesh properties were found to yield mesh converging results for the outputs of the study.

Regarding the discretization order, the thermal analysis uses linear shape functions; notice that the membranes are not included in the thermal analysis. In the mechanical analysis, all triangular elements in the containment structure and rock are assigned quadratic shape function, while the tendon membranes are assigned linear shape functions. This in order to have quadratic displacement and linear strain variation for both elements since the membranes includes rotational degrees of freedom. The mesh of the axisymmetric cross-section is shown in Figure 4-2a with a more detailed picture of one of the tendon membranes shown Figure 4-2b in a swept configuration. A summary of the number of element and reference to the element type in Abaqus [6] is given in Table 4-1. The difference in the number of elements used in the containment structure in the thermal and mechanical analysis is due to a few added internal geometry boundaries in the mechanical model that affects the mesh algorithm. This does not, however, affect the results since the temperature varies linearly in all domains.

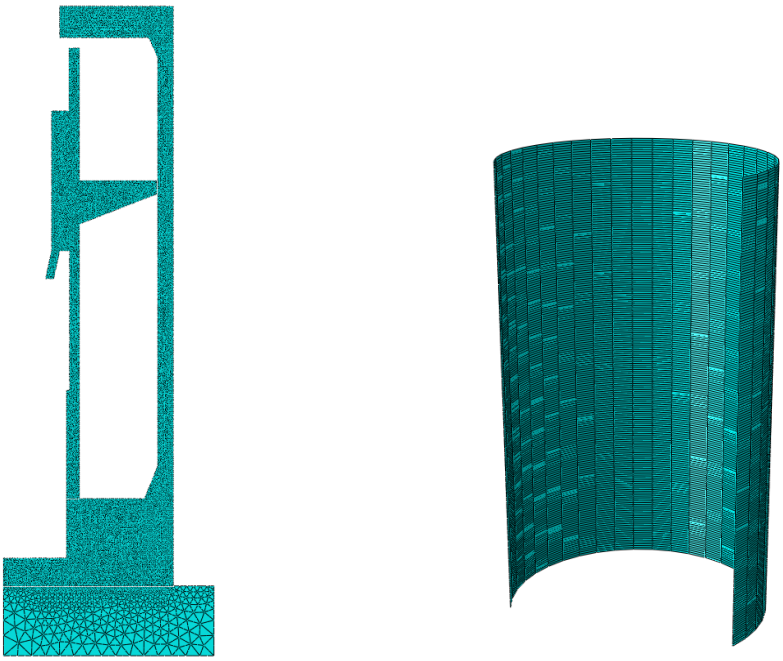

a) b)

Figure 4-2: *Finite element mesh used in the mechanical analysis: containment plus rock (a) and swept representation of one of the tendon membranes (b).*

Table 4-1: *Summary of the used FE mesh in the axisymmetric model.*

Analysis	Domain	Reference	Number of elements
Thermal	Rock	DCAX3	761
	Containment	DCAX3	8390
Mechanical	Rock	CAX6M	761
	Containment	CAX6M	9525
	Tendons	MAX1	402

4.4 RESULTS

4.4.1 Thermal

The distribution of temperature induced within the axisymmetric model is presented in Figure 4-3 for assumed external temperatures according to Figure 2-5b.

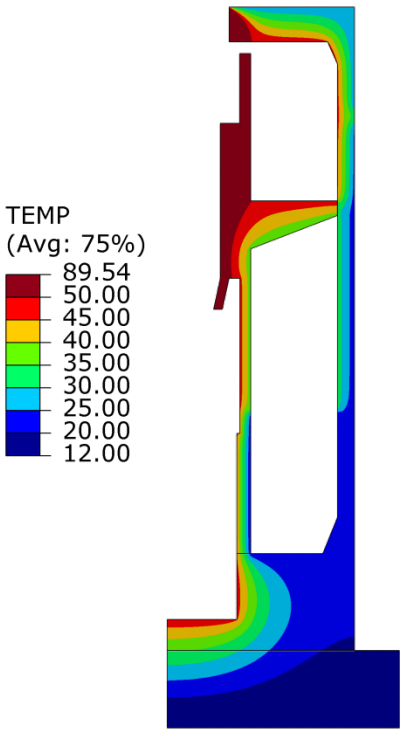

Figure 4-3: *Calculated temperature distribution based on ambient temperature from Figure 2-5.*

4.4.2 Mechanical

For each of the six load steps in the mechanical analysis described in Section 3.3.3, the magnitude of displacements is presented in Figure 4-4.

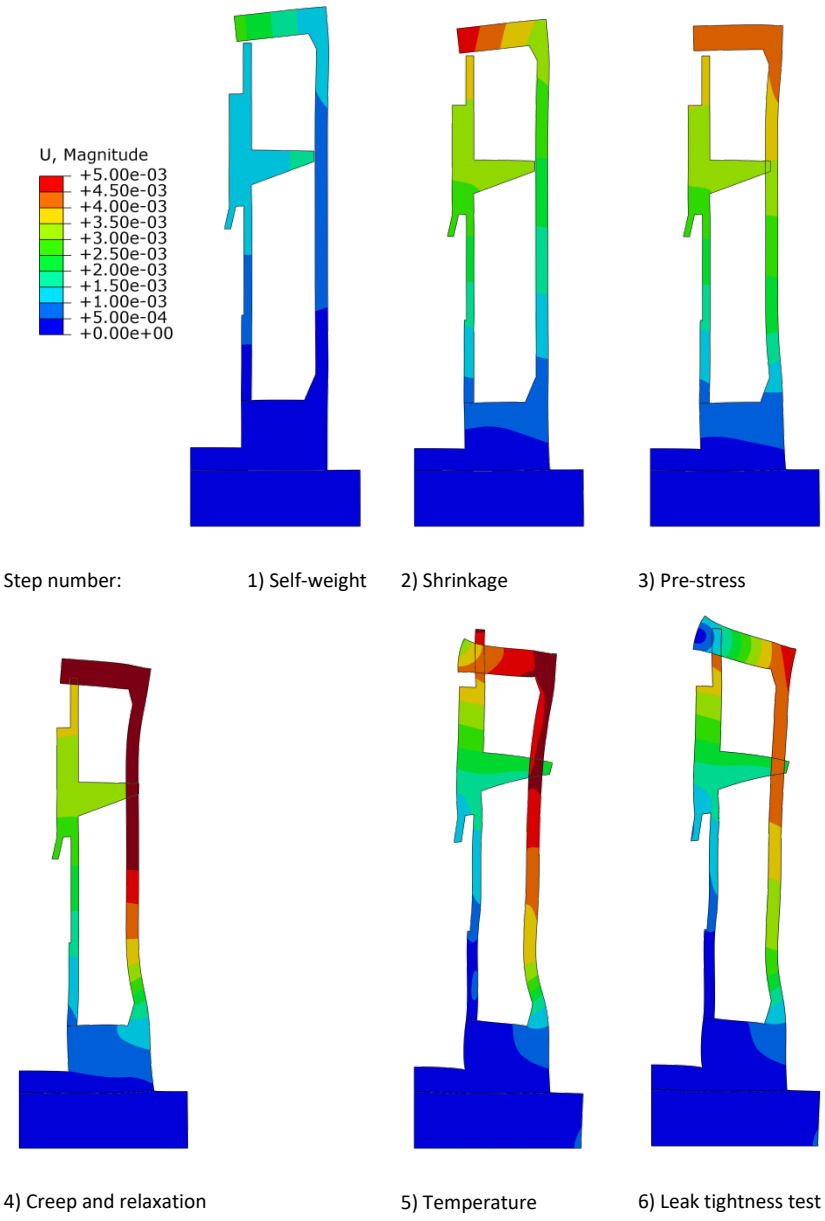

Figure 4-4: *Deformed sate of the containment at the end of every analysis sequence (step number). Note that deformations are scaled by a factor 1000.*

The vertical and radial displacements from the simulation are shown in Figure 4-5 for each load step at the lower gusset (+4.6 m), mid-height (+18.5 m), the intermediate slab (+25 m) and the upper gusset (+33.8 m). The simulated vertical and hoop strains on the outside surface of the containment wall at the same locations are shown in Figure 4-6.

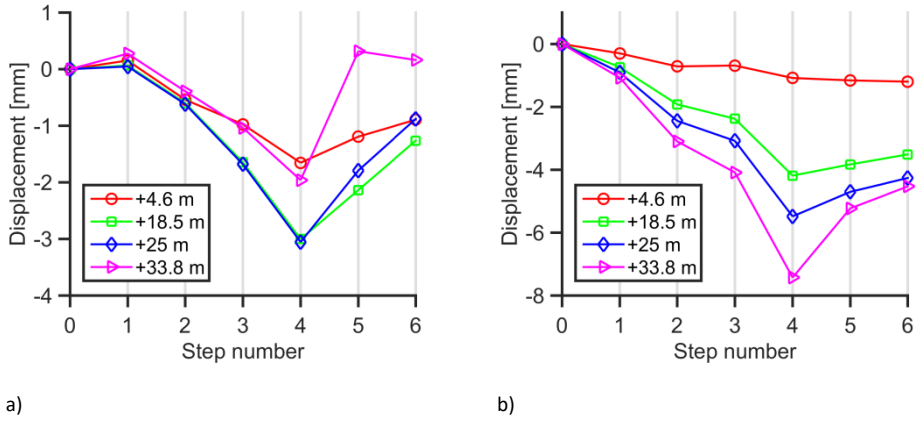

Figure 4-5: *Radial displacement (a) and vertical displacement (b) at three different heights in the containment wall. Values plotted at the end of each analysis step.*

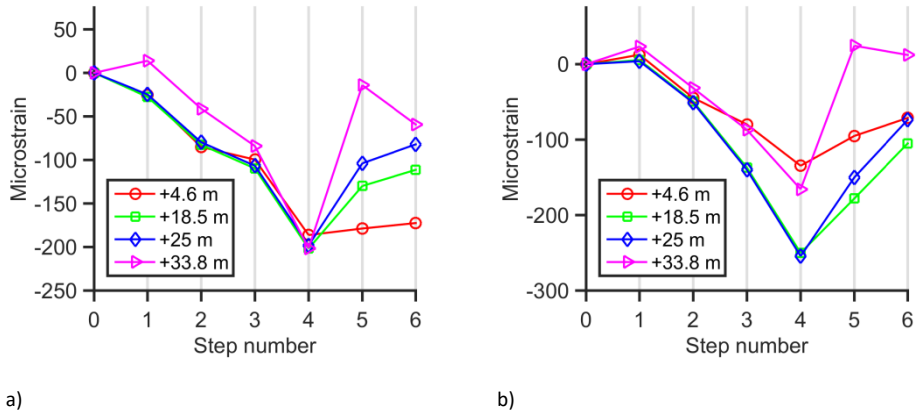

Figure 4-6: *Vertical (a) and hoop (b) strain on the outer surface of the containment wall at three different heights. Values are plotted at the end of each analysis step and show the total strain.*

The simulated change in the gap between the inner concrete structure and the containment wall is shown in Figure 4-7. A positive change distance means that the two absolute gap between the two structure have decreased.

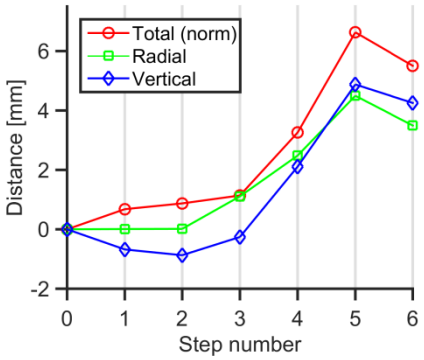

Figure 4-7: *Change in distance between the inner structure and the containment wall. Values plotted at the end of each analysis step.*

The simulated mean stress in the tendons including long-term losses is shown in Figure 4-8 at four heights. It should be noted that the forces from the horizontal tendons have been assumed constant over the height in the axi-symmetric model. According to Section 2.1.1, the total force in vertical and horizontal direction is 14400 MP and 16600 MP respectively. Divided by the total area of tendons in the vertical and horizontal direction gives average stresses equal to 1001 MPa and 655 MPa respectively. This corresponds well with the presented stresses in Figure 4-8.

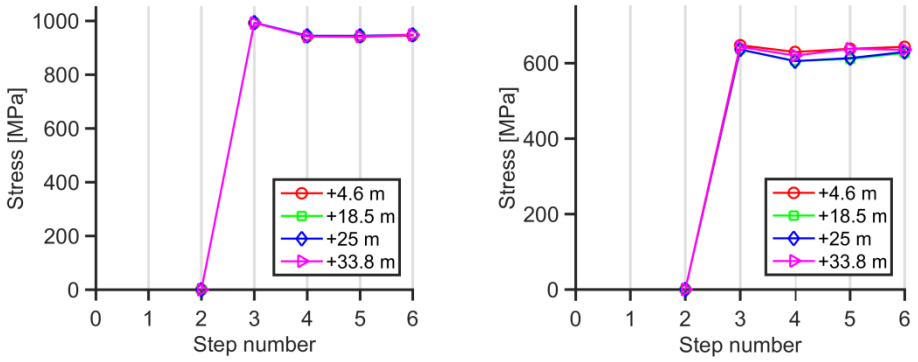

a) b)

Figure 4-8: *Normal stress in vertical (a) and hoop (b) tendons at three different heights. Values plotted at the end of each analysis step.*

5 Ring model

As mentioned in Section 3, to study the three-dimensional deformation of the outer containment wall, a slice of the wall is modelled using FE model. The model is constructed as a ring. Two segments were cut from the outer concrete containment wall height; the elevation of the upper surface was +24.00 m and +13.75 m, see Figure 4-1. The results of the analysis presented in this section compared and evaluated with the asymmetrical model.

5.1 GEOMETRY

The main dimensions of the ring model are taken from the report [3] and complemented with some measurements from drawings provided during the project. For modelling, a 1.8 m high ring segment of concrete containment wall was selected. A ring of 1.1 m thick and two buttresses, where the hoop tendons are anchored, are modelled. Notice that no other details such as reinforcement and the steel liner are included in the modeol.

The ring is pre-stressed by eight and six horizontal at level +24.00 and +13.75 respectively. The horizontal tendons are placed in two layers with the radius 11.7 m and 11.9 m for the inner and outer layers, respectively. Fifty-two vertical tendons are placed at a radius of 11.8 m. In addition, twelve vertical tendons are placed at buttresses, six tendons on each side, see Figure 5-1. The total cross-sectional area of one tendon is 0.002 m^3, in both horizontal and vertical directions. Based on the provided drawings, the vertical spacing between the horizontal tendons is 0.45 m and 0.60 m at level +24.00 m and +13.75 m, respectively. The distribution of vertical tendons is varying, with closely spaced tendons at the area without buttresses. For simplicity, it was assumed that the 52 vertical tendons distributed with constant spacing at a radius of 11.8 m.

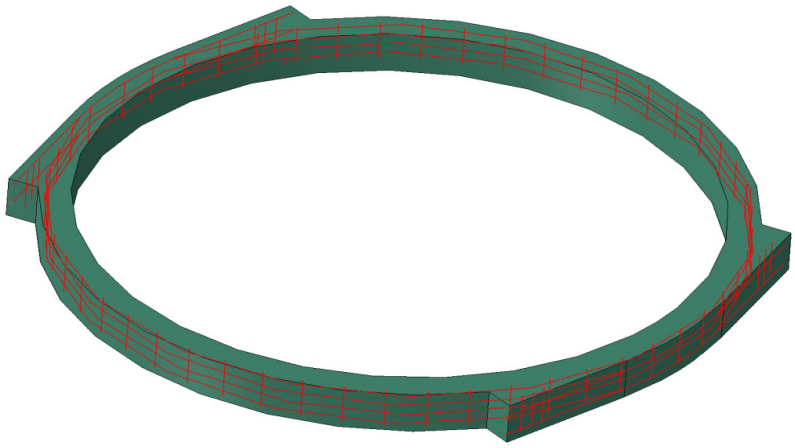

Figure 5-1: *Layout of tendons in the ring model.*

5.2 BOUNDARY CONDITIONS AND LOADS

5.2.1 Thermal

As mention in Section 4.2.1, the temperature boundaries are defined using Eq. (3-2).

5.2.2 Mechanical

Boundary conditions

The model is constrained in radial and vertical directions across the lower surface of the concrete ring while its tangential motions are enabled.

External loads

The applied external loads are listed below; their background is described in Section 2.3. All loads are applied during the self-weight (1) as described in Section 3.3.3, except the internal pressure.

- Self-weight of the dome and wall above the +24.00 m level was modelled as pressure of 0.8 MPa applied to the upper surface of the ring
- Pressure test – Internal pressure of 3 bar applied to all surfaces inside the containment

Internal loads

As mention in Section 4.2.2, the temperature is taken from the thermal analysis to calculate the thermal strains ε_{th} needed in the constitutive equations presented in Section 3.3.

The instantaneous strain ε_{pi} needed in constitutive equation (3-10) for the tendons in the respective tendon direction is calculated as:

$$\varepsilon_{pi,v} = \frac{F_{v,tot}}{A_v E_s} = \frac{14400 \cdot 9810}{0.1411 \cdot 210\text{e}9} = 0.0048 \qquad (5\text{-}1)$$

$$\varepsilon_{pi,h} = \frac{F_{h,tot}}{A_h E_s} = \frac{2034 \cdot 9810}{0.016 \cdot 210\text{e}9} = 0.0058 \qquad (5\text{-}2)$$

where the forces $F_{v,tot}$ and $F_{h,tot}$ are taken as the average forces without considering long-term losses. Also, using the equation from EC2 [4] presented in appendix A to calculate the loss in pre-stress due to relaxation in needed Eq. (3-10) yields:

$$\Delta\sigma_{pr,v} = 29.6 \text{ MPa} \qquad (4\text{-}5)$$

$$\Delta\sigma_{pr,h} = 74.6 \text{ MPa} \qquad (5\text{-}6)$$

As already discussed in Section 3.3.1, the compressive stress σ_c needed in Eq. (3-6) is estimated from the FE analysis and taken as an approximate stress in the containment wall directly after the post-tensioning. Given the different amounts of pre-stress in the vertical and horizontal directions two stresses are taken from the model:

$$\sigma_{c,v} = 2.5 \text{ MPa} \quad (5\text{-}3)$$

$$\sigma_{c,h} = 5.1 \text{ MPa} \quad (5\text{-}4)$$

resulting in different amounts of creep for the respective direction. To this end, it must be emphasized that these are approximate stresses that are assumed uniform in the entire wall. In the simulation, as well as in reality stresses in the containment wall not uniform due to its deformation, temperature and shrinkage effects. However, stresses due to the pre-stress are dominating and the approximation should give satisfactory results for the purpose of this study.

5.3 MESH

The concrete containment, the structure is discretized using hexahedral solid elements with second-order shape functions and an approximate size of 0.3 m. The tendons are discretized with elements of the same size.

In the mechanical analysis, all hexahedral elements in the concrete ring are assigned quadratic shape function, while the tendons are assigned as truss elements with linear shape functions. The mesh is shown in Figure 4-2. A summary of the number of element and reference to the element type in Abaqus [6] is given in Table 4-1.

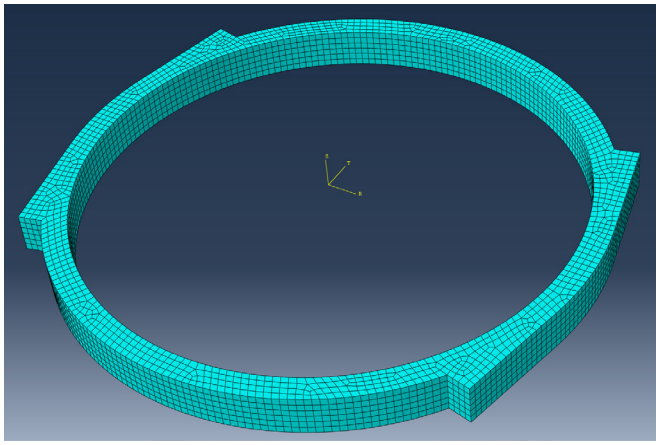

Figure 5-2: *Finite element mesh used in the mechanical analysis: concrete containment ring*

Table 5-1: *Summary of the used FE mesh in the ring model.*

Analysis	Domain	Reference	Number of elements
Thermal	Containment	DCAX3	6672
Mechanical	Containment	C3D8	6672
	Tendons	T3D2	1520

5.4 RESULTS

5.4.1 Thermal

The distribution of temperature induced within the ring model is presented in Figure 5-3. The maximum temperature acting on concrete containment in real working condition was found to be 50 °C and 20 °C, inside and outside the concrete containment, respectively.

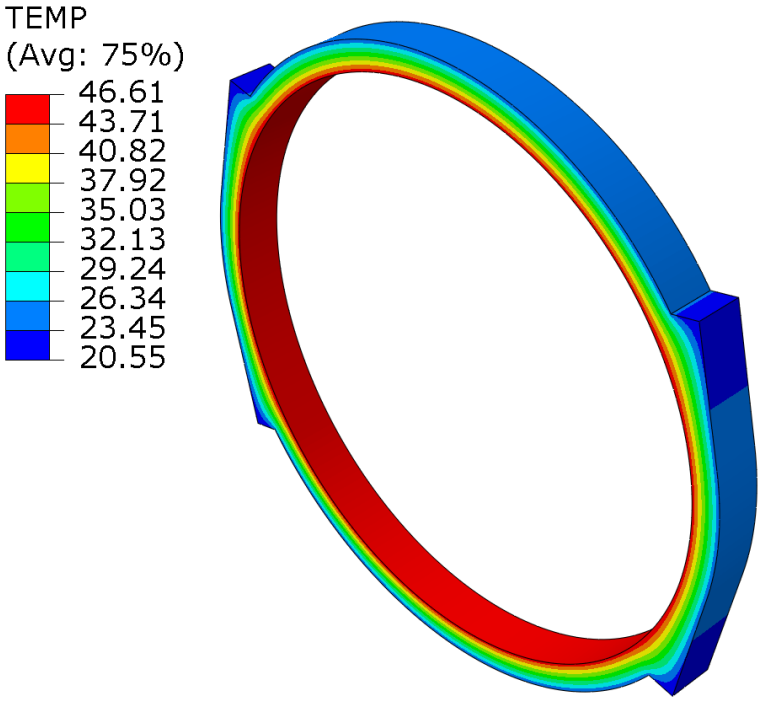

Figure5-3: *Calculated temperature distribution based on ambient temperature from Figure 2-5.*

5.4.2 Mechanical

For each of the six load steps the magnitude displacement is presented in Figure 5-4.

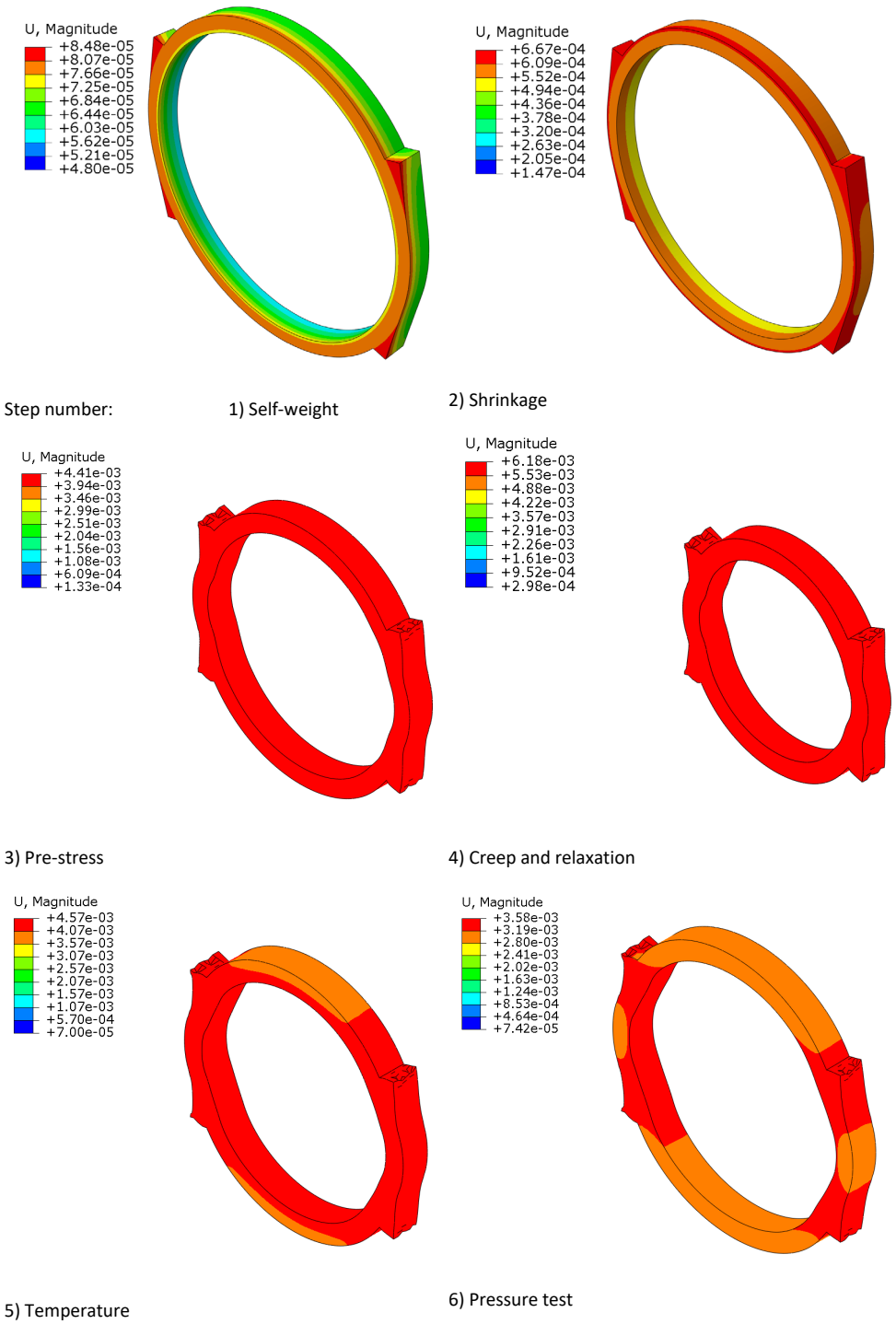

Figure 5-4: *Deformed sate of the containment at the end of every analysis sequence (step number) at +24.00 m. Note that deformations are scaled by a factor 1000.*

The radial displacement and hoop strains at five different angles: 0°, 45°, 54°, 70°and 90°, for two models (i.e. +24.00 m and +13.75 m) are presented in Figure 5-5 and Figure 5-6, respectively. The analysis results, for example in Figure 5-6, using a three-dimensional finite element ring model are a little larger than that those using an axisymmetric model; i.e. Figure 4-5.

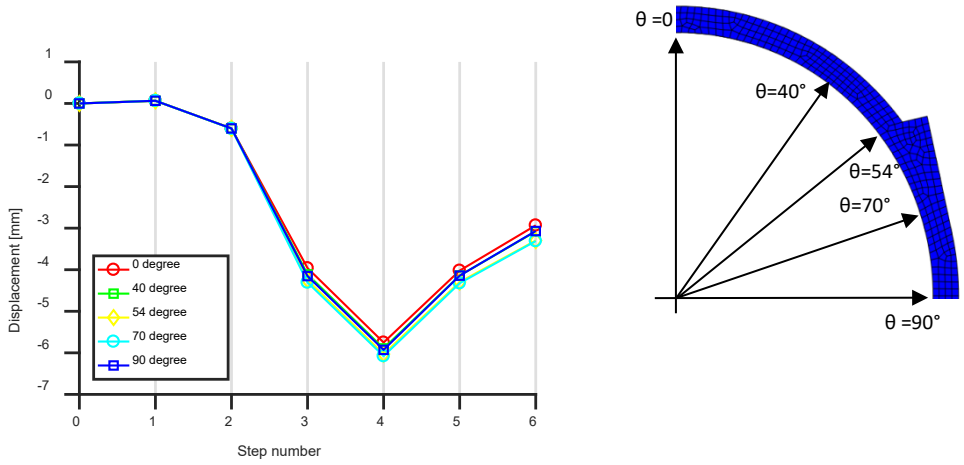

a)

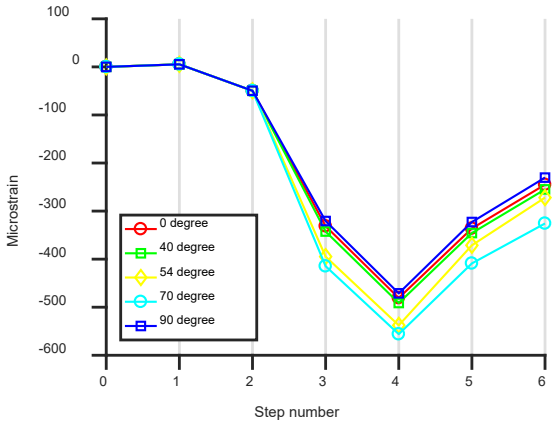

b)

Figure 5-5: *Radial displacement (a) and hoop strain (b) at five different angles in the containment ring at level +24.00 m. Values plotted at the end of each analysis step.*

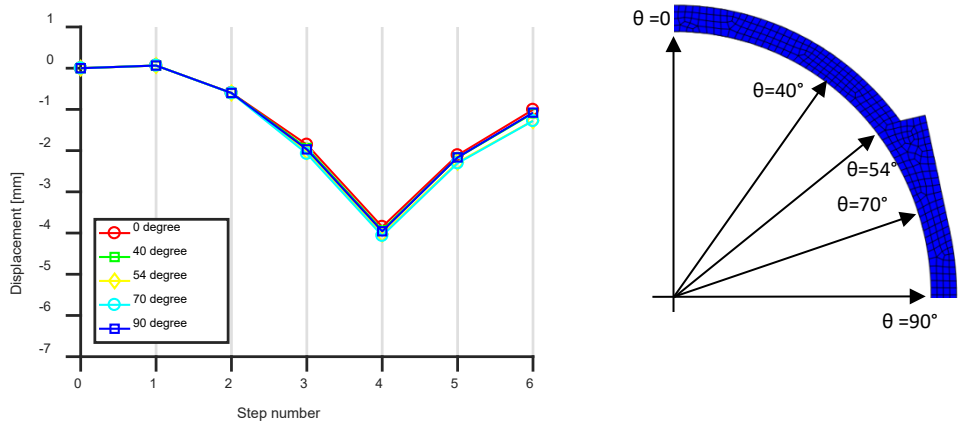

a)

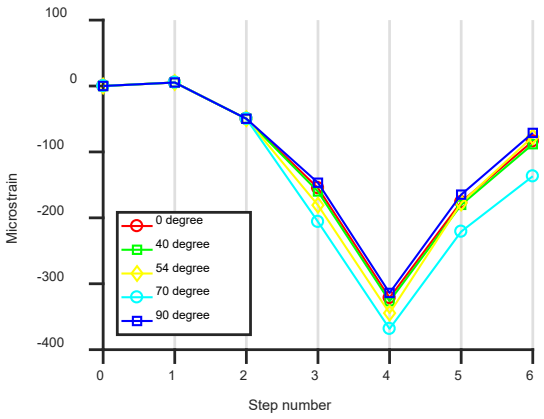

b)

Figure 5-6: *Radial displacement (a) and hoop strain (b) at five different angles in the containment ring at level +13.75 m. Values plotted at the end of each analysis step.*

The simulated stress in the tendons including losses is shown in Figure 4-8.

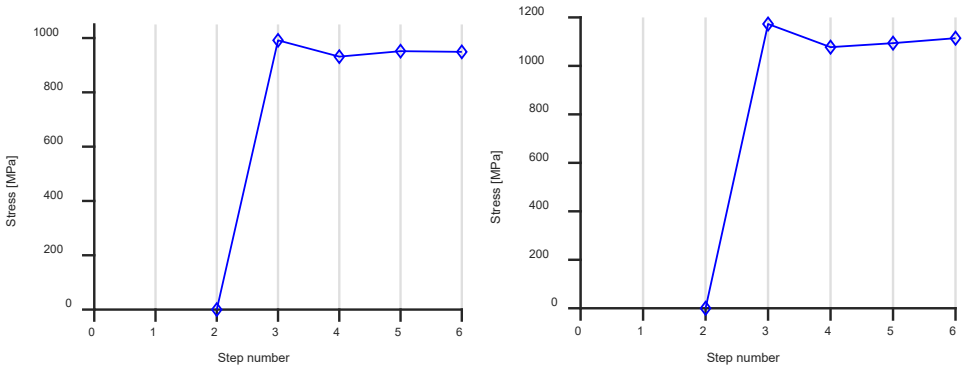

a) b)

Figure 5-6: *Normal stress in vertical (a) and hoop (b) tendons. Values plotted at the end of each analysis step.*

6 Instrumentation

Based on the analyses of the axisymmetric model and the ring model, a recommendation regarding the level of instrumentation is given. The basis for this recommendation is to suggest as few sensors as possible that still is included some redundancy. In addition, the majority of the sensors should be installed on the outside of the cylinder wall to minimize radioactive contamination and for easier installation and tendon drawings. Finally, the suggested placement of the sensors is based on the fact that it should be easy to access. Thereby limit the need for permanent scaffolding to be built to access the sensors (which may be needed for calibration etc.).

The types of sensors have been divided into two categories; *detectors* and *support instrumentation*. The detectors are measuring key aspects of the structural response and could be used along with alarm values. The intention with the support instrumentation is that it provides information that is needed as input for numerical analyses etc.

6.1 DETECTORS

One of the most important parameters to measure is the displacement of the containment wall. The displacement of the containment wall is highly influenced by the stiffness of the structure and thereby the pre-stressing of the tendons. In the vertical section it is recommended that the displacement is measured at four levels

- Upper gusset (just below the variation in thickness of the gusset).
- Intermediate slab (at the level for the bottom slab in the upper drywell)
- Mid height of the cylinder wall
- Lower gusset (just above the variation in thickness of the gusset)

In addition, these deformations should be measured on at least three points along the perimeter. By measuring these displacements on three points in the plane it is possible to capture effects if any uneven deformation occurs. It is suggested that these points are located as follows

- One point in the centre of the cylinder, between the two anchoring positions for tendons (0 °)
- Two points located just next to the anchoring of tendons (130° & 230°)

The suggested placements of sensors for measuring the displacement are illustrated in Figure 6-1.

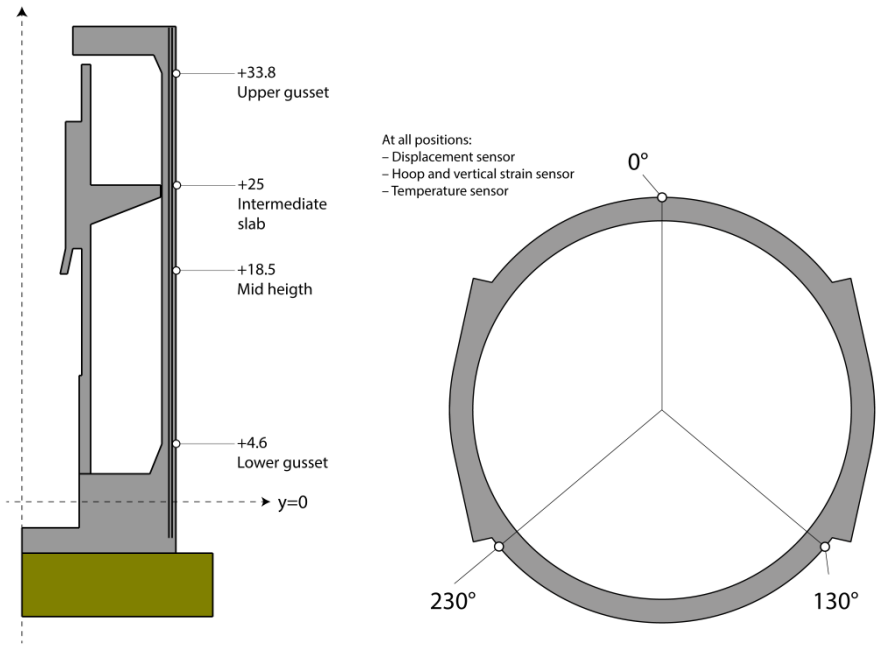

a) b)

Figure 6-1: *Suggested instrumentation shown in a vertical cross-section (a) and a horizontal cross-section.*

The displacement can, for instance, be measured with hanging pendulums with automatic (3D) registration of the displacement. In an automated optical measurement of the displacement of the wire, a resolution of about 0.01 mm is expected with accuracy less than 0.1 mm, according to [8].

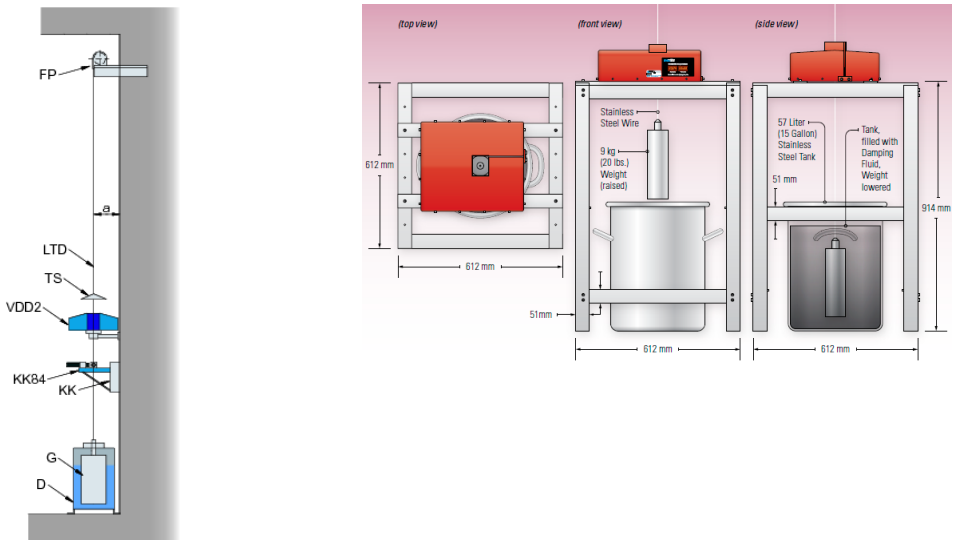

a) b)

Figure 6-2 *Examples of a hanging pendulum (a)[1] and a system for automatic registration (b)[2].*

[1] http://www.huggenberger.com/en/measuring-devices-for/changes-in-inclination-and-displacement/direct-pendulum-gl.html
[2] http://www.geokon.com/BGK-6850A

In close connection to these points, the vertical and hoop strain should also be measured. The strain can typically be measured with strain gauges, as illustrated in Figure 6-3.

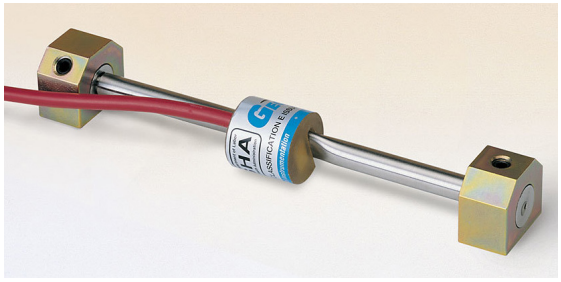

Figure 6-3 *Example of a strain gauge*[3].

It is recommended that temperatures are measured with the same sensor as the strain gauge or in close proximity to be able to adjust for thermal expansion of the sensor. Many strain gauges, such as the example shown in Figure 6-3, measures both strain and temperature. The resolution for this type of sensor is about 1_με. The accuracy about 0.5 % in the range 3000_με for standard calibration, but can be about 0.1 % with individual calibration, i.e. 15 or 3 με for standard or individual calibration, [9]. In this case, individual calibration is required, considering the expected variations in strain shown in Table 6-1.

Based on the numerical analyses, the estimated approximate recordings for sensors during a pressure test are summarized. Based on these values it is possible to determine the suitable resolution of the sensors. It should be noted that due to long term effects, the measuring range of the sensors should be significantly higher than the values presented in this table.

Table 6-1: *Estimated relative response during 3 bar pressure test at different positions.*

Height/polar coordinate	Radial disp.	Vertical disp.	Vertical strain	Hoop strain
+4.6 m	0.30 mm	0.04 mm	$6.25*10^{-6}$	$23.9*10^{-6}$
+18.5 m	0.87 mm	0.32 mm	$45.2*10^{-6}$	$73.0*10^{-6}$
+25 m	0.91 mm	0.44 mm	$18.6*10^{-6}$	$76.4*10^{-6}$
+33.8 m	0.15 mm	0.70 mm	$21.8*10^{-6}$	$12.2*10^{-6}$
0° at +24 m	1.1 mm	-	-	$91.2*10^{-6}$
130°/230° at +24 m	1.0 mm	-	-	$99.2*10^{-6}$

In addition to these sensors, displacement sensors between the intermediate slab and the cylinder wall measuring their relative radial displacement should also be included at the positions shown in Figure 6-1b. Unlike the other sensors, these sensors are installed inside the concrete containment. In addition to these, displacement sensors measuring the relative displacement between the biological shield and the roof are also an important location inside the containment to monitor. This should also be made at the same locations as the shown in Figure 6-1b.

[3] http://www.geokon.com/4000

The suggested amount of sensors that are given corresponds to a lower limit of sensors that should be used to capture the behaviour of the containment. This does, however, include some redundancy, which may be needed to detect possible errors with sensors or to be able to capture the structural response even if a few sensors would malfunction.

6.2 SUPPORT INSTRUMENTATION

In addition to the sensors needed for verification of the structural response during pressurization tests (i.e. the detectors), additional support sensors may be required that gives input needed for numerical analyses.

In this report all ambient temperatures had to be assumed, with more temperature input values more correct predictions can be made. The assumed temperatures used in these analyses are shown in Figure 6-4. The ambient temperature values for each of these thermal regions should be measured. This could for example be done by the combined strain-temperature sensors shown in Figure 6-3. The temperature range for these types of sensors is about -20 to +80 °C, with an accuracy of 0.5 °C or 0.1 °C for standard and individual calibration respectively. Furthermore, the internal temperature of the concrete should be measured, but then mainly for verification purposes.

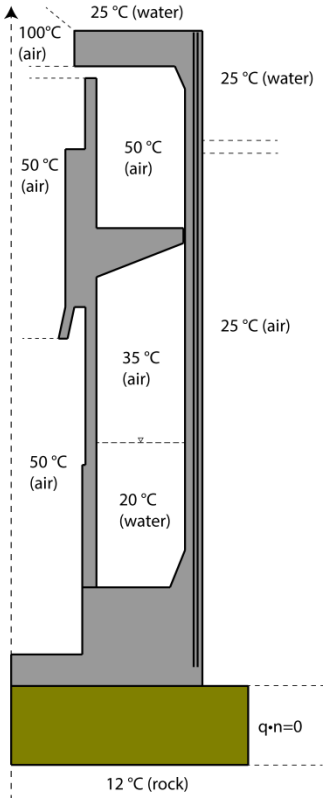

Figure 6-4 Assumed temperatures

In addition, in this case an epoxy coating had been placed on the containment walls which prevent water transport and thereby drying shrinkage. It is likely that the coating could have some defects which would result in some extent of drying shrinkage. Therefore, it is suitable to also measure the relative humidity.

The design methods, such as Eurocode, are based on the ambient relative humidity and therefore this should primarily be measured. The relative humidity does only have to be measured on the outside of the concrete containment (the placement of the steel liner prevents water transport). It is therefore suggested that relative humidity sensors are installed close to the other sensors (strain gauges etc.). Relative humidity sensors should be installed measuring the ambient relative humidity for the different climatic zones for the containment building, see for instance Figure 6-4.

For verification purposes, it is also recommended that a few relative humidity sensors are installed in the containment wall, drilled from the outside. These should be installed close to the ambient relative humidity sensors, and installed at three different depths within the containment wall. The measurements performed by Oxfall [10] showed a moisture profile according to Figure 6-5. Example of suitable sensors to use are for instance given in [7]. Similar results were also shown in the Nugenia/Acceppt project for a PWR containment, see [11]. The relative humidity should according to this, preferably be measured at the distances 100 mm, 200 mm and 300 mm from the exterior surface of the containment wall.

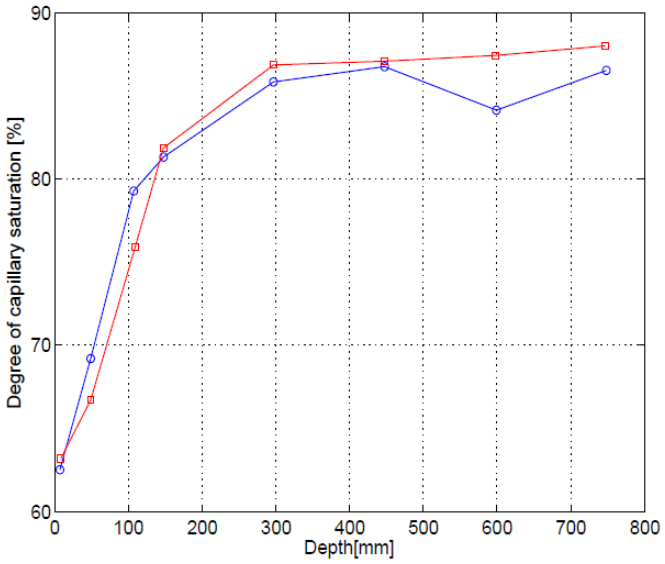

Figure 6-5 Example of moisture profile in a concrete containment wall, from Oxfall et al. (2014)

6.3 SAMPLING

In general, with all types of measurements it recommended to use higher sampling frequency than needed for the evaluation in order to allow for filtering of background noise etc. For this type of slow occurring events, a sampling frequency of about 1 to 5 minutes is considered sufficient and is detailed enough to be used for post-processing (filtering, down-sampling etc.).

7 Summary and conclusions

Nuclear concrete containment buildings typically consist of pre-stressed concrete, where pre-stressing tendons are utilized to enforce a compressive state of stress to ensure that cracks do not occur in the containment structure. These tendons are in some cases cement grouted to reduce the risk of corrosion. However, this results in that it is not possible to directly measure the current tendon force.

One conventional method to assess the status of the containment building, and thereby indirectly the tendons, is to perform pressure tests. The response of the containment can after this be determined based on measurements of displacements and strains.

In this project, numerical analyses have been used to simulate a pressure test of a Boiling Water Reactor (BWR) that is common in Sweden and Finland. In this case, the model is based information given by TVO on Olkiluoto 2. Based on these simulations, the response of the containment building is determined and suggestions are made regarding suitable placement of measuring sensors.

The suggested instrumentation has been divided into different types of sensors defined as detectors and support sensors. The detectors are needed to monitor the structural response of the containment while the support sensors are needed to give sufficient input to numerical analyses.

It is suggested that detector sensors are placed at four vertical positions and at three points along the perimeter. At these locations, it is recommended that displacement sensors, strain gauges and temperature sensors are installed.

In addition, it is also recommended that the relative radial displacements between the intermediate slab and the cylinder wall and the relative displacement between the biological shield and the roof are monitored.

After the review of this report was made, experimental results from OL 2 (which now has a similar measuring system as the one suggested in this report) were made available by the curtesy of TVO.

In Table 7-1, the measured results made available are presented along with the corresponding values from the FE analysis. As it can be seen in the table, the simplified models used in this project are in fairly good agreement. It is important to remember that the purpose of this project was only to estimate a reasonable range of the measured values for the purpose to see what kind of measuring devices could be used to capture the expected response.

As it can be seen, the simplified models are in close agreement in the measured behaviour in the radial direction. The agreement in the vertical direction is not as good, but still within the correct range.

Table 7-1 Comparison between measured and calculated response.

Height/polar coordinate	Position	Direction	Pendulum (mm)	FE-model (mm)
+18.5 m	0 °	Radial displacement	-0.85	-0.87
+18.5 m	0 °	Vertical displacement	-0.54	-0.32

The simplified models thereby performed even better than expected in this project. The reason for the discrepancies between numerical models and measured response may of course be due to the assumptions made in the project. It indicates that for later stages of this project, when the purpose is detailed validation the behaviour of a numerical model and calibration with measurements (in order to estimate the status condition of the tendons and the containment building), then more sophisticated 3 D models may be required.

8 Bibliography

[1] T. Roth, J. Silfwerbrand and H. Sundquist, "Betonginneslutningar i svenska kärnkraftverk," SKI Report 02:59, Statens kärnkraftsinspektion SKI, Stockholm, 2002.

[2] USNCR, "Regulatory Guide 1.90 - Inservice inspection of prestressed concrete containment structures with grouted tendons," U.S Nuclear Regulatory Commission, 1977.

[3] MMI Engineering, "OL1& OL2 Containment Dynamic Analysis Models and Modal Analysis CONTANA Project," MMI Engineering, Inc, Oakland, 2012.

[4] CEN, "Eurocode 2: Design of concrete structures – Part 1-1: General rules and rules for buildings," CEN, 2004.

[5] M. Könönen, "Temperature induced stresses in a reactor containment building: A case study of Forsmark F1," KTH Royal Institute of Technology, Stockholm, 2012.

[6] Abaqus, *Abaqus 6.14 Online Documentation*, Providence, USA: Dassault Systmes, 2014.

[7] T. Gasch, R. Malm and A. Ansell, "A coupled hygro-thermo-mechanical model for concrete subjected to variable environmental conditions," *International Journal of Solids and Structures*, vol. 91, pp. 143-156, 2016.

[8] Geokon, "Pendelum System, Model BGK-6850A.," 2017. [Online]. Available: http://www.geokon.com/BGK-6850A. [Accessed 22 09 2017].

[9] Geokon, "Strain Gauges, Model 4000.," 2017. [Online]. Available: http://www.geokon.com/4000. [Accessed 22 09 2017].

[10] M. Oxfall, P. Johansson and M. Hassanzadeh, "Moisture profiles in concrete walls of a nuclear reactor containmen after 30 years of operation.," in *Nordic Concrete Research - Proceedings of XXII Nordic Concrete Symposium.*, Reykjavik, 2014.

[11] D. Eriksson, R. Malm and H. Hansson, "NUGENIA ACCEPPT G3.2 – Analysis of stress concentrations and crack risk," KTH, Stockholm, 2015.

Appendix A: Creep, shrinkage, pre-stress and relaxation

ASSUMPTIONS

- The concrete is assumed to have a mean compressive strength after 28 days of 40 MPa.
    - Other relevant material parameters are calculated based on formulas given in the Eurocode [4]
- Pre-tensioning (and thus start of creep) is assumed to occur one year after casting
- No influence of ambient relative humidity due to moisture tight epoxy barrier. Hence, RH=100 % is assumed in all subsequent equations.

CROSS-SECTIONAL DATA

The creep and shrinkage model in EC2 utilize cross-sectional data to determine the evolution of shrinkage and creep strains. This is, however, mainly used to account for the influence of ambient relative humidity and should have little effect for the current application. Nonetheless, for completeness the needed cross-sectional data is estimated.

First the cross-sectional area A_c is needed, which is here calculated for a unit height of 1 m and a wall thickness of 0.8 m:

$$A_c = 1 \cdot 1.1 = 1.1 \text{ m}^2$$

Next, the perimeter of the member in contact with the atmosphere u_c is needed. Here, both the inside and outside surfaces of the wall is taken into to consideration. Note that the moisture tight barrier is later accounted for by setting RH=100 %.

$$u_c = 2 \cdot 1.1 = 2.2 \text{ m}$$

Finally, the notational size of the cross-section h_c is calculated:

$$h_c = 2 \cdot A_c / u_c = 1.0 \text{ m}$$

which is equal to the unit height assumed.

CREEP STRAINS

Creep strains are calculated using Eq. (3-6) in which the creep ratio $\varphi(t, t_0)$ is needed. Following the EC2 model:

$$\varphi(t, t_0) = \varphi_{RH} \beta_{fcm} \beta_{t0} \beta_c(t, t_0)$$

where the factors controlling the amount of creep are calculated as:

$$\varphi_{RH} = \left[1 + \frac{1 - \mathrm{RH}}{0.1\sqrt[3]{h_0}}\left(\frac{35}{f_{cm}}\right)^{0.7}\right]\left(\frac{35}{f_{cm}}\right)^{0.2} = \left[1 + \frac{1 - 1}{0.1\sqrt[3]{1}}\left(\frac{35}{40}\right)^{0.7}\right]\left(\frac{35}{40}\right)^{0.2} = 0.974$$

$$\beta_{fcm} = \frac{16.8}{\sqrt{f_{cm}}} = \frac{16.8}{\sqrt{40}} = 0.42$$

$$\beta_{t0} = \frac{1}{(0.1 + {t_0}^{0.2})} = \frac{1}{(0.1 + 365^{0.2})} = 3.07$$

The last factor (β_c) controls the time-dependence of the creep and is for $t = 35$ years calculated as:

$$\beta_c = \left(\frac{t - t_0}{\beta_H + t - t_0}\right)^{0.3} = \left(\frac{35 \cdot 365 - 365}{1403 + 35 \cdot 365 - 365}\right)^{0.3} = 0.968$$

The value of β_c varies between 0 to 1, hence it can be concluded that after 35 years almost all creep have occurred given a constant stress. Notice that the factor β_H is dependent on the relative humidity, notational size and the compressive strength:

$$\beta_H = \min\left\{1.5\left[1 + \left(\frac{0.012\mathrm{RH}}{100}\right)^{18}\right]h_0 + 250\left(\frac{35}{f_{cm}}\right)^{0.5}, 1500\left(\frac{35}{f_{cm}}\right)^{0.5}\right\}$$
$$= \min\left\{1.5\left[1 + \left(\frac{0.0121}{100}\right)^{18}\right]1 + 250\left(\frac{35}{40}\right)^{0.5}, 1500\left(\frac{35}{40}\right)^{0.5}\right\} = 1403$$

The creep ratio after 35 years is thus:

$$\varphi(t, t_0) = \varphi_{RH}\beta_{fcm}\beta_{t0}\beta_c(t, t_0) = 0.974 \cdot 0.42 \cdot 3.07 \cdot 0.968 = 1.217$$

SHRINKAGE STRAINS

Given RH=100 % drying shrinkage is set to zero. Hence, the total shrinkage is given by the autogenous shrinkage calculated according to Eq. (3-8). The asymptotic value of shrinkage is in the EC2 model calculated as:

$$\varepsilon_{ca} = 2.5(f_{cm} - 18) \cdot 10^{-6} = 2.5(40 - 18) \cdot 10^{-6} = 55 \cdot 10^{-6}$$

The factor β_{as} that controls the time evolution is for $t = 35$ years calculated as:

$$\beta_{as} = 1 - \exp\left(-0.2\sqrt{t}\right) = 1 - \exp\left(-0.2\sqrt{35 \cdot 365}\right) = 1$$

which means that all autogenous shrinkage h occurred. Looking at intermediate values of β_{as}, 98 % of the autogenous shrinkage has occurred after 1 year. This justifies the assumption that all shrinkage occurs before post-tensioning as described in section 3.3.3.

PRE-STRESS

Modelling of the instantaneous strain ε_{pi} due to post-tensioning different for the two models and described in sections 4 and 5, respectively.

RELAXATION STRAINS

Also losses will be different for the two models since the loss is dependent on the amount of stress in the tendons. For a pre-stress $\sigma_{pi} = E_s\,\varepsilon_{pi}$ losses due to relaxation in the tendons are calculated using Eq. (3-11) where the loss in pre-stress $\Delta\sigma_{pr}$ is calculated as proposed in the EC2 [4].

$$\frac{\Delta\sigma_{pr}}{\sigma_{pi}} = 0.66\rho_{1000}\exp\left(0.91\frac{\sigma_{pi}}{f_{yk}}\right)\left(\frac{t-t_0}{1000}\right)^{0.75\left(1-\frac{\sigma_{pi}}{f_{yk}}\right)}10^{-5}$$

$$= 0.66\cdot 2.5\exp\left(0.91\frac{\sigma_{pi}}{1500}\right)\left(\frac{35\cdot 365-365}{1000}\right)^{0.75\left(1-\frac{\sigma_{pi}}{1500}\right)}10^{-5}$$

INSTRUMENTATION AND MODELLING OF A REACTOR CONTAINMENT BUILDING

The most important safety barrier in a nuclear power plant is the reactor containment, a post-tensioned concrete structure enclosing the reactor.

The pre-stressing tendons prevent cracking of the concrete in case of a reactor accident, why the tension in the tendons is crucial to the integrity of the reactor containment. The tendon forces decrease over time, so to ensure the integrity of the reactor containment, it is important to monitor the tendon forces.

This report suggests an instrumentation system of the reactor containment for the Finnish nuclear power plant Olkiluoto 2, for measuring the global and local deformations of the structure, moisture and temperature. The system could be used for continuous long-term measurements and during the periodic pressure tests.

Energiforsk is the Swedish Energy Research Centre – an industrially owned body dedicated to meeting the common energy challenges faced by industries, authorities and society. Our vision is to be hub of Swedish energy research and our mission is to make the world of energy smarter!

Energiforsk